

Neutralino Dark Matter in the USSM

J. Kalinowski^{1,2}, S.F. King³ and J.P. Roberts^{1,4}

¹*Physics Department, University of Warsaw, 00-681 Warsaw, Poland*

²*Theory Division, CERN, CH-1211 Geneva 23, Switzerland*

³*School of Physics and Astronomy, University of Southampton,
Southampton, SO17 1BJ, U.K.*

⁴*Center for Cosmology and Particle Physics, New York University,
New York, NY 10003, USA*

Abstract

This paper provides a comprehensive discussion of neutralino dark matter within classes of extended supersymmetric models referred to as the USSM containing one additional SM singlet Higgs plus an extra Z' , together with their superpartners the singlino and bino'. These extra states of the USSM can significantly modify the nature and properties of neutralino dark matter relative to that of the minimal (or even next-to-minimal) supersymmetric standard models. We derive the Feynman rules for the USSM and calculate the dark matter relic abundance and direct detection rates for elastic scattering in the USSM for interesting regions of parameter space where the largest differences are expected.

1 Introduction

One of the benefits of weak scale supersymmetry (SUSY) with conserved R parity is that the lightest supersymmetric particle (LSP) is absolutely stable, and provides a weakly interacting massive particle (WIMP) candidate [1, 2] capable of accounting for the observed cold dark matter (CDM) relic density $\Omega_{CDM}h^2 = 0.1099 \pm 0.0062$ [3]. In particular, the lightest neutralino in SUSY models is an excellent candidate, providing its mass, composition and interactions are suitably tuned to result in the correct value of $\Omega_{CDM}h^2$. The minimal supersymmetric standard model (MSSM) has become a widely studied paradigm [4]. However the stringent upper bound on the Higgs boson mass in the MSSM combined with its experimental lower bound from LEP has led to some tension in the electroweak symmetry breaking sector, roughly characterized by a fine-tuning of parameters at the percent level [5]. While the experimental elusiveness of the Higgs boson may cast some doubt on the MSSM, there are a host of non-minimal SUSY models which predict a heavier and/or more weakly coupled Higgs boson [4].

A further reason to move beyond the minimal case is the so-called mu problem of the MSSM [6]. The MSSM contains a bilinear mass term that couples the two Higgs doublets with a dimensionful coupling μ . This term is SUSY preserving, and as such only has two natural values, $\mu = 0$ and $\mu = M_{Pl}$ (unless special forms of the Kahler metric are assumed). However experimental data and the stability of the Higgs mass requires that μ be of the order of the SUSY breaking scale. In non-minimal SUSY models the mu problem is solved by setting $\mu = 0$ and including an additional superfield \hat{S} , a singlet under the Standard Model (SM) gauge group, which couples to the Higgs doublet superfields \hat{H}_1, \hat{H}_2 according to $\lambda \hat{S} \hat{H}_1 \hat{H}_2$, where λ is a dimensionless coupling constant. We shall refer to such models generically as singlet SUSY models. Such a coupling replaces the SUSY Higgs/Higgsino mass term $\mu \hat{H}_1 \hat{H}_2$ of the MSSM. The singlet vacuum expectation value (TeV) $\langle S \rangle$ then dynamically generates a SUSY Higgs/Higgsino mass near the weak scale as required. This results in an increased Higgs boson mass upper bound depending on the value of λ , and hence a welcome reduction in electroweak fine tuning in addition to solving the μ problem of the MSSM [7].

However, although an extra singlet superfield \hat{S} seems like a minor modification to the MSSM, which does no harm to either gauge coupling unification or neutralino dark matter, there are further costs involved in this scenario since the introduction of the singlet superfield \hat{S} leads to an additional accidental global $U(1)_X$ (Peccei-Quinn (PQ) [8]) symmetry which will result in a weak scale massless axion when it is spontaneously broken by $\langle S \rangle$ [9]. Since such an axion has not been observed experimentally, it must be removed somehow. This can be done in several ways resulting in different non-minimal SUSY models, each involving additional fields and/or parameters. For example, the classic solution to this problem is to introduce a singlet term \hat{S}^3 , as in the next-to-minimal supersymmetric standard model (NMSSM) [10], which reduces the PQ symmetry to the discrete symmetry Z_3 . The subsequent breaking of a discrete symmetry at the weak

scale can lead to cosmological domain walls which would overclose the Universe. This can be avoided by breaking the Z_3 symmetry explicitly without upsetting the hierarchy problem by non-renormalizable operators that obey a Z_2 R -symmetry [11], or by removing the \hat{S}^3 term altogether [12].

Another solution to the axion problem of singlet models, which we follow, is to promote the PQ symmetry to an Abelian $U(1)_X$ gauge symmetry [13]. The idea is that the extra gauge boson will eat the troublesome axion via the Higgs mechanism resulting in a massive Z' at the TeV scale. The essential additional elements of such a scenario then consist of two extra superfields relative to those of the MSSM, namely the singlet superfield \hat{S} and the $U(1)_X$ gauge superfield B' . The scenario involving only the MSSM superfields plus these two additional superfields, may be considered as a phenomenological model in its own right which has been referred to as the USSM. In the USSM, then, the MSSM particle spectrum is extended by a new CP-even Higgs boson S , a gauge boson Z' and two neutral -inos: a singlino \tilde{S} and a bino' \tilde{B}' while other sectors are not enlarged. The presence of new singlino and bino' states greatly modifies the phenomenology of the neutralino sector both at colliders and in cosmology-related processes. The collider phenomenology and cosmology of the USSM has been studied in [14, 15, 16, 17, 18, 19, 20], which we briefly review as follows.

The collider phenomenology of the USSM has recently been considered in [18]. The neutralino production cross sections and their decay branching fractions depend crucially on their masses and composition with respect to the MSSM case. If the new -ino states are heavy, their influence on the MSSM neutralinos is small. In contrast, if the singlino mass scale is low, the production rates can be quite different and, since there are more neutralinos, the decay chains of sparticles can be longer. Moreover, if the mass gaps between the MSSM and new -inos are very small, the standard decay modes are almost shut and radiative transitions between neutralino states with a soft photon may be dominant. In such a case the decay chains can be apparently shorter, a feature which is of relevance for the LHC experiments.

The dark matter phenomenology of the USSM was first studied in [15, 16], and more recently in [19]. In [15], the analysis was performed in a scenario with a very light Z' and considered the case in which the LSP was a very light singlino. This allowed the authors to consider the annihilation of dark matter in the early universe to be dominated by s-channel Z' processes, allowing an analytic solution to the dark matter relic density to be obtained. In the full parameter space of the USSM, this is just one possibility, and indeed such a light Z' is heavily disfavored by current data. In [19] the recoil detection of the dark matter candidate in the USSM (and other non-minimal SUSY models) was considered.

In this paper, we provide an up to date and comprehensive analysis of neutralino dark matter in the USSM¹. We provide a complete discussion of the extended gauge,

¹The recent observation of a positron excess by the PAMELA collaboration [21] have caused a flurry

neutralino, Higgs squark and slepton sectors in the USSM, and using the LanHEP [24] package, derive all the new Feynman rules involving these extended sectors. We first provide a complete qualitative discussion of the new annihilation channels relevant for the calculation of the cold dark matter relic density for the neutralino LSP in the USSM. We also discuss the elastic scattering cross section for the neutralino LSP in the USSM, including both spin-independent and spin-dependent parts of the cross sections, relevant for the direct dark matter search experiments. We then survey the parameter space of the USSM, and discuss quantitatively how the nature and composition of the neutralino LSP can be significantly altered compared to that in the MSSM due to the extra singlino and bino' states, for different ranges of parameters. The Feynman rules are then implemented into the micrOMEGAs [25] package in order to calculate the relic density for the corresponding regions of parameter space. This provides a full calculation of the annihilation channels including co-annihilation and careful treatment of resonances as well as accurately calculating the relic density for an arbitrary admixture of states. In this way we extend the analysis of USSM neutralino dark matter annihilation beyond the specific cases previously studied in the literature. We also perform an equally general calculation of the direct detection cross-sections for USSM dark matter for elastic neutralino–nuclei scattering.

It is worth emphasizing that the USSM is not a complete model, since from its definition it does not include the additional superfields at the TeV scale, charged under the gauged Abelian symmetry, which are necessarily present in order to cancel the fermionic gauge anomalies involving the $U(1)_X$ gauge symmetry. For example, a well motivated and elegant solution to the problem of anomaly cancelation is to identify the Abelian gauge group as a subgroup of E_6 and then cancel the anomalies by assuming complete 27 dimensional representations of matter down to the TeV scale. With the further requirement that the right-handed neutrino carries zero charge under the Abelian gauge group (in order to have a high scale see-saw mechanism) this then specifies the theory uniquely as the E_6 SSM [26, 27]. However our working assumption is that the additional matter superfields required to cancel anomalies are heavy compared to the Z' mass. The USSM considered in this paper may thus be regarded as a low-energy truncation of the E_6 SSM model, with other E_6 SSM fields assumed heavy, and the charge assignments under the extra $U(1)_X$ as given in [27] and summarized in Section 2.

Despite that fact that the USSM must be regarded as a truncation of a complete model, it makes sense to study the physics and cosmology in the USSM since it provides a simplified setting to learn about crucial features which will be relevant to any complete model involving an additional $U(1)_X$ gauge group and a singlet. For example, as already mentioned the neutralino LSP in the USSM may have components of the extra gaugino

of speculation that the high energy positrons are produced by annihilating dark matter in the galactic halo[22]. An alternative explanation is that astrophysical sources could account for the positron excess - in particular nearby pulsars [23]. It is unclear as yet which of these explanations is correct and as a result we do not address the PAMELA results further in this work.

\tilde{B}' and singlino \tilde{S} , in addition to the usual MSSM neutralino states. Naively we might expect that the dark matter phenomenology of such regions would be similar to that of singlino dark matter in the NMSSM. However this is not the case. The inclusion of the bino' state, as well as the lack of a cubic interaction term \hat{S}^3 , results in a significant change in the phenomenology. Also the neutralino mass spectrum in the USSM is very different from that of the NMSSM as the singlino mass is determined indirectly by a mini-see-saw mechanism involving the bino' soft mass parameter M'_1 rather than through a diagonal mass term arising from the cubic \hat{S}^3 . The lack of a cubic interaction term also restricts the annihilation modes of the singlino, making it dominantly reliant on annihilations involving non-singlet Higgs bosons and higgsinos. As the USSM has a different Higgs spectrum to the NMSSM, notably in the pseudoscalar Higgs sector, the Higgs dominated annihilation channels of the USSM singlino are significantly modified with respect to the NMSSM singlino. As Higgs exchange diagrams dominate the direct detection phenomenology, the difference in the Higgs spectrum and the singlino interactions results in significant differences in the direct detection predictions as well.

The remainder of the paper is organized as follows. In section 2 we shall define the Lagrangian of the USSM and discuss the Higgs, Z' , neutralino and sfermion sectors. In sections 3 and 4 we shall give an overview of the important features of the relic density calculation and the direct detection calculation, respectively, highlighting the main differences to the MSSM. In section 5 we present the results of the full numerical calculations for both the relic density and the direct detection cross-section. It will be performed in two physically interesting scenarios: (A) with the MSSM higgsino and gaugino mass parameters fixed, while the mass of the extra U(1) gaugino taken free (to complement the collider phenomenology discussed in Ref. [18]); (B) with GUT-unified gaugino masses. Section 6 summarizes and concludes the paper. The mass matrix structure of the extended Higgs scalar sector, and a discussion of the Feynman rules involving the extended neutralino sector in the USSM are given in a pair of appendices.

2 The USSM model

Including the extra $U(1)_X$ symmetry, the gauge group of the model is $G = SU(3)_C \times SU(2)_L \times U(1)_Y \times U(1)_X$ with the couplings g_3, g_2, g_Y, g_X , respectively. In addition to the MSSM superfields, the model includes a new vector superfield \hat{B}_X and a new iso-singlet Higgs superfield \hat{S} . The usual MSSM Yukawa terms \hat{W}_Y of the MSSM superpotential (*i.e.* without the μ term) are augmented by an additional term that couples the iso-singlet to the two iso-doublet Higgs fields:

$$\hat{W} = \hat{W}_Y + \lambda \hat{S} (\hat{H}_u \hat{H}_d). \quad (1)$$

The coupling λ is dimensionless. Gauge invariance of the superpotential \hat{W} under $U(1)_X$ requires the $U(1)_X$ charges to satisfy $Q_{H_d}^X + Q_{H_u}^X + Q_S^X = 0$ and corresponding relations

between the $U(1)_X$ charges of Higgs and matter fields. In the following we adopt the $U(1)_X$ charges as in the E_6 SSM model [27], see Table 1. (For notational convenience we will also use $Q_1 = Q_{H_d}^X$, $Q_2 = Q_{H_u}^X$ and $Q_S = Q_S^X$.) The effective μ parameter is generated by the vacuum expectation value $\langle S \rangle$ of the scalar S -field.

i	Q	u^c	d^c	L	e^c	N^c	S	H_2	H_1
$\sqrt{\frac{5}{3}}Q_i^Y$	$\frac{1}{6}$	$-\frac{2}{3}$	$\frac{1}{3}$	$-\frac{1}{2}$	1	0	0	$\frac{1}{2}$	$-\frac{1}{2}$
$\sqrt{40}Q_i^X$	1	1	2	2	1	0	5	-2	-3

Table 1: *The $U(1)_Y$ and $U(1)_X$ charges of matter fields in the USSM, where Q_i^X and Q_i^Y are defined with the correct E_6 normalization factor required for the RG analysis [27].*

The USSM particle content, in addition to the MSSM particles, includes a single extra scalar state, a new Abelian gauge boson and an additional neutral higgsino and gaugino state. The chargino sector remains unaltered, while the sfermion scalar potential receives additional D-terms.

2.1 The Abelian gauge sector

With two Abelian gauge factors, $U(1)_Y$ and $U(1)_X$, the two sectors can mix through the coupling of the kinetic parts [28],

$$\mathcal{L}_{\text{gauge}} = \frac{1}{32} \int d^2\theta \left\{ \hat{W}_Y \hat{W}_Y + \hat{W}_X \hat{W}_X + 2 \sin \chi \hat{W}_Y \hat{W}_X \right\}, \quad (2)$$

where \hat{W}_Y and \hat{W}_X are the corresponding chiral superfields. The gauge/gaugino part of the Lagrangian can be converted back to the canonical form by the $GL(2, \mathbb{R})$ transformation from the original superfield basis \hat{W}_Y, \hat{W}_X to the new one $\hat{W}_B, \hat{W}_{B'}$ [28, 29]:

$$\begin{pmatrix} \hat{W}_Y \\ \hat{W}_X \end{pmatrix} = \begin{pmatrix} 1 & -\tan \chi \\ 0 & 1/\cos \chi \end{pmatrix} \begin{pmatrix} \hat{W}_B \\ \hat{W}_{B'} \end{pmatrix}. \quad (3)$$

This transformation alters the $U(1)_Y \times U(1)_X$ part of the covariant derivative to

$$D_\mu = \partial_\mu + ig_Y Y_i B_\mu + i(-g_Y Y_i \tan \chi + \frac{g_X}{\cos \chi} Q_i^X) B'_\mu \quad (4)$$

$$= \partial_\mu + ig_1 Y_i B_\mu + ig'_1 Q'_i B'_\mu, \quad (5)$$

where we introduced the notation $g_1 = g_Y$, $g'_1 = g_X / \cos \chi$. We will also use $g' = g_1 \sqrt{3/5}$ for the low-energy (non-GUT normalized) hypercharge gauge coupling.

With the above mixing matrix the hypercharge sector of the Standard Model is left unaltered, while the effective $U(1)_X$ charge is shifted from its original value Q_i^X to

$$Q'_i = Q_i^X - \frac{g_1}{g'_1} Y_i \tan \chi. \quad (6)$$

As a result of the kinetic mixing, new interactions among the gauge bosons and matter fields are generated even for matter fields with zero $U(1)_X$ charge.

In the E_6 SSM the two $U(1)$ gauge groups are automatically orthogonal at the GUT scale and the RG running effects give acceptable small mixing at the low scale [27, 30] providing in a natural way the general agreement between SM analyses and precision data [31]. Therefore in the remainder of the paper we will simply write Q_i instead of Q'_i .

After breaking the electroweak and $U(1)_X$ symmetries spontaneously due to non-zero vacuum expectation values of the iso-doublet and the iso-singlet Higgs fields,

$$\langle H_u \rangle = \frac{\sin \beta}{\sqrt{2}} \begin{pmatrix} 0 \\ v \end{pmatrix}, \quad \langle H_d \rangle = \frac{\cos \beta}{\sqrt{2}} \begin{pmatrix} v \\ 0 \end{pmatrix}, \quad \langle S \rangle = \frac{1}{\sqrt{2}} v_S, \quad (7)$$

the Z, Z' mass matrix takes the form

$$M_{ZZ'}^2 = \begin{pmatrix} M_Z^2 & \Delta^2 \\ \Delta^2 & M_{Z'}^2 \end{pmatrix}, \quad (8)$$

where

$$\begin{aligned} M_Z^2 &= \frac{g'^2 + g_2^2}{4} v^2 \\ \Delta^2 &= \frac{g'_1 \sqrt{g'^2 + g_2^2}}{2} v^2 (Q_1 \cos^2 \beta - Q_2 \sin^2 \beta) \\ M_{Z'}^2 &= g_1^2 v^2 (Q_1^2 \cos^2 \beta + Q_2^2 \sin^2 \beta) + g_1^2 Q_S^2 v_S^2 \end{aligned} \quad (9)$$

We then diagonalise the mass matrix to give the mass eigenstates:

$$\begin{pmatrix} Z_1 \\ Z_2 \end{pmatrix} = D_{ij} \begin{pmatrix} Z \\ Z' \end{pmatrix} = \begin{pmatrix} \cos \alpha_{ZZ'} & \sin \alpha_{ZZ'} \\ -\sin \alpha_{ZZ'} & \cos \alpha_{ZZ'} \end{pmatrix} \begin{pmatrix} Z \\ Z' \end{pmatrix} \quad (10)$$

where the resultant masses and ZZ' mixing angle are given by

$$M_{Z_1, Z_2}^2 = \frac{1}{2} \left(M_Z^2 + M_{Z'}^2 \mp \sqrt{(M_Z^2 - M_{Z'}^2)^2 + 4\Delta^4} \right) \quad (11)$$

$$\alpha_{ZZ'} = \frac{1}{2} \arctan \left(\frac{2\Delta^2}{M_{Z'}^2 - M_Z^2} \right) \quad (12)$$

2.2 The Higgs sector

In the charged sector it is convenient to introduce the G^\pm, H^\pm basis as:

$$\begin{aligned} G^- &= H_d^- \cos \beta - H_u^{+*} \sin \beta \\ H^+ &= H_d^{-*} \sin \beta + H_u^+ \cos \beta \end{aligned} \quad (13)$$

After the gauge symmetry breaking, two Goldstone modes G^\pm from the original H_u and H_d doublets are eaten by W^\pm fields leaving two physical charged Higgs bosons H^\pm , with the mass

$$m_{H^\pm}^2 = \frac{\sqrt{2}\lambda A_\lambda}{\sin 2\beta} v_S - \frac{\lambda^2}{2} v^2 + \frac{g_2^2}{2} v^2 + \Delta_\pm, \quad (14)$$

where the trilinear coupling A_λ is the soft-SUSY breaking counterpart of λ , and the one-loop corrections Δ_\pm are the same as in the MSSM [32] with the effective μ parameter given by

$$\mu \equiv \lambda \frac{v_S}{\sqrt{2}}.$$

In the CP-conserving model the CP-even and CP-odd scalar Higgs component fields do not mix. The CP-even sector involves $\text{Re } H_d^0$, $\text{Re } H_u^0$ and $\text{Re } S$ fields. The 3×3 mass matrix of the CP-even Higgs scalars M_{even}^2 has been calculated to one-loop in Refs. [27, 33] in the field space basis h, H, S . This basis² is rotated by an angle β with respect to the interaction basis,

$$\sqrt{2} \text{Re} \begin{pmatrix} H_d^0 \\ H_u^0 \\ S \end{pmatrix} = \begin{pmatrix} \cos \beta & -\sin \beta & 0 \\ \sin \beta & \cos \beta & 0 \\ 0 & 0 & 1 \end{pmatrix} \begin{pmatrix} h \\ H \\ N \end{pmatrix} + \begin{pmatrix} v \cos \beta \\ v \sin \beta \\ v_S \end{pmatrix} \quad (15)$$

The explicit form of M_{even}^2 is given in Appendix A. It can be diagonalized by a 3×3 orthogonal mixing matrix (\mathcal{O}), i.e.

$$M_H^{2 \text{diag}} = \mathcal{O}^T M_{even}^2 \mathcal{O} \quad (16)$$

by going to the mass eigenstates basis

$$(H_1, H_2, H_3) = (h, H, N) \mathcal{O} \quad (17)$$

in which, by convention, mass eigenstates are ordered by mass, $m_{H_i} \leq m_{H_{i+1}}$.

It will be convenient to introduce a mixing matrix \mathcal{O}' ,

$$\mathcal{O}' = \begin{pmatrix} \cos \beta & -\sin \beta & 0 \\ \sin \beta & \cos \beta & 0 \\ 0 & 0 & 1 \end{pmatrix} \mathcal{O}, \quad (18)$$

that enters the Feynman rules. It is a superposition of two rotations in eqs. (15) and (17) and links the interaction eigenstates H_d^0, H_u^0, S directly to the CP-even mass eigenstates H_1, H_2, H_3 .

²Note that h, H are not the MSSM-like eigenstates.

The imaginary parts of the neutral components of the Higgs doublets and Higgs singlet compose the CP-odd sector of the model. In the field basis A, G, G' defined by

$$\begin{aligned}\sqrt{2} \operatorname{Im} H_d^0 &= G \cos \beta + (A \cos \phi - G' \sin \phi) \sin \beta \\ \sqrt{2} \operatorname{Im} H_u^0 &= -G \sin \beta + (A \cos \phi - G' \sin \phi) \cos \beta \\ \sqrt{2} \operatorname{Im} S &= A \sin \phi + G' \cos \phi\end{aligned}\tag{19}$$

the massless pseudoscalar G, G' fields are absorbed to Z, Z' after the electroweak gauge symmetry breaking. The physical CP-odd Higgs boson A acquires mass

$$m_A^2 = \frac{\sqrt{2}\lambda A_\lambda}{\sin 2\phi} v + \Delta_{EA}\tag{20}$$

where $\tan \phi = v \sin 2\beta / 2v_S$ and the one-loop correction Δ_{EA} is given in Appendix A.

Note that the Higgs sector of this model involves only one physical CP-odd pseudoscalar as in the MSSM, since, unlike the NMSSM, the extra CP-odd state arising from the singlet is eaten by the Z' . However, there are three CP-even scalars, one more than in the MSSM, where the extra singlet state arises from the extra singlet as in the NMSSM. The characteristic Higgs mass spectrum in this model is governed by the value of λ . For small values of λ , say $\lambda < g_1$, the Higgs spectrum resembles that of the MSSM, with the heaviest CP-even Higgs scalar being predominantly composed of the singlet scalar state, and being approximately degenerate with the CP-odd pseudoscalar and the charged Higgs states when their masses exceed about 500 GeV. In this regime the lightest CP-even Higgs scalar is Standard Model like, and respects the MSSM mass bound. On the other hand, for large values of λ , say $\lambda > g_1$, a viable Higgs mass spectrum only occurs for a very large CP-odd Higgs mass, say $m_A \approx 2 - 3$ TeV, with the heaviest CP-even Higgs scalar being non-singlet and degenerate with the CP-odd and charged Higgs states. The second heaviest Higgs scalar is comprised mainly of the singlet state and is thus unobservable, while the lightest CP-even Higgs scalar is Standard Model like but may significantly exceed the MSSM bound. For more details concerning the Higgs sector see [27].

2.3 The neutralino sector

The Lagrangian of the neutralino system follows from the superpotential in Eq. (1), complemented by the gaugino $SU(2)_L$, $U(1)_Y$ and $U(1)_X$ mass terms of the soft-supersymmetry breaking electroweak Lagrangian:

$$\mathcal{L}_{\text{mass}}^{\text{gaugino}} = -\frac{1}{2}M_2\tilde{W}^a\tilde{W}^a - \frac{1}{2}M_Y\tilde{Y}\tilde{Y} - \frac{1}{2}M_X\tilde{X}\tilde{X} - M_{YX}\tilde{Y}\tilde{X} + \text{h.c.}\tag{21}$$

where the \tilde{W}^a ($a = 1, 2, 3$), \tilde{Y} and \tilde{X} are the (two-component) $SU(2)_L$, $U(1)_Y$ and $U(1)_X$ gaugino fields, and M_i ($i = 2, X, Y, YX$) are the corresponding soft-SUSY breaking mass

parameters. After performing the transformation of gauge superfields to the gauge boson eigenstate basis, Eq.(3), the Lagrangian takes the form

$$\mathcal{L}_{\text{mass}}^{\text{gaugino}} = -\frac{1}{2}M_2\tilde{W}^a\tilde{W}^a - \frac{1}{2}M_1\tilde{B}\tilde{B} - \frac{1}{2}M'_1\tilde{B}'\tilde{B}' - M_K\tilde{B}\tilde{B}' + \text{h.c.}, \quad (22)$$

where

$$M'_1 \equiv \frac{M_X}{\cos^2\chi} - \frac{2\sin\chi}{\cos^2\chi}M_{YX} + M_Y \tan^2\chi, \quad M_K \equiv \frac{M_{YX}}{\cos\chi} - M_Y \tan\chi, \quad (23)$$

and we introduce the conventional notation for the U(1) bino mass $M_1 \equiv M_Y$. In parallel to the gauge kinetic mixing discussed in Sect.2.1, the Abelian gaugino mixing mass parameter M_{YX} is assumed small compared with the mass scales of the gaugino and higgsino fields.

Notice that the gauge kinetic term mixing (and the corresponding soft-SUSY breaking mass) can be a source of mass splitting between the \tilde{B} and \tilde{B}' gauginos in models with universal gaugino masses $M_X = M_Y$. Since the mixing angle χ must be small, as required by data [31], the splitting is very small. The splitting could be enhanced if additional U(1) gauge factors in the hidden sector were present that mix via the kinetic term with the visible sector.³ In our phenomenological analyses, therefore, we will consider two scenarios: (A) with M'_1 taken as a free parameter, independent from M_1 ; and (B) with M'_1 tight to M_1 and M_2 by a unification of gaugino masses at the GUT scale.

After breaking the electroweak and U(1)_X symmetries spontaneously the doublet higgsino mass μ and the doublet higgsino–singlet higgsino mixing μ_λ parameters are generated

$$\mu \equiv \lambda \frac{v_S}{\sqrt{2}} \quad \text{and} \quad \mu_\lambda \equiv \lambda \frac{v}{\sqrt{2}}. \quad (24)$$

The USSM neutral gaugino–higgsino mass matrix in a basis of two–component spinor fields $\xi \equiv (\tilde{B}, \tilde{W}^3, \tilde{H}_d^0, \tilde{H}_u^0, \tilde{S}, \tilde{B}')^T$ can be written in the following block matrix form

$$M_{\tilde{\chi}^0} = \left(\begin{array}{cccc|cc} M_1 & 0 & -M_Z c_\beta s_W & M_Z s_\beta s_W & 0 & M_K \\ 0 & M_2 & M_Z c_\beta c_W & -M_Z s_\beta c_W & 0 & 0 \\ -M_Z c_\beta s_W & M_Z c_\beta c_W & 0 & -\mu & -\mu_\lambda s_\beta & Q_1 g'_1 v c_\beta \\ M_Z s_\beta s_W & -M_Z s_\beta c_W & -\mu & 0 & -\mu_\lambda c_\beta & Q_2 g'_1 v s_\beta \\ \hline 0 & 0 & -\mu_\lambda s_\beta & -\mu_\lambda c_\beta & 0 & Q_S g'_1 v_S \\ M_K & 0 & Q_1 g'_1 v c_\beta & Q_2 g'_1 v s_\beta & Q_S g'_1 v_S & M'_1 \end{array} \right) \quad (25)$$

³Since the fields in the hidden sector are generally considered to be heavy enough and the hidden-visible mixing is expected to be small, their effect on the visible gauge sector can be negligible. Nevertheless, the mass of the Abelian gaugino in the visible sector can obtain a substantial contribution, as advocated in [34].

where the upper-left 4×4 is the neutral gaugino–higgsino mass matrix of the MSSM, the lower-right 2×2 corresponds to the new sector containing the singlet higgsino (singlino) and the new $U(1)$ –gaugino \tilde{B}' that is orthogonal to the bino \tilde{B} , and off-diagonal 4×2 describes the coupling of the two sectors via the neutralino mass matrix ($s_\beta \equiv \sin \beta$, $c_\beta \equiv \cos \beta$, and s_W, c_W are the sine and cosine of the electroweak mixing angle θ_W). Notice the see-saw type structure of the new sector due to the absence of a diagonal mass parameter for the singlino \tilde{S} , which is in direct contrast to the NMSSM in which the cubic self-interaction generates a singlet mass term[10]. For the same reason, in the USSM the lightest neutralino can never be bino'-dominated.

In general, the neutralino mass matrix $M_{\tilde{\chi}^0}$ is a complex symmetric matrix. To transform this matrix to the diagonal form, we introduce a unitary 6×6 matrix N such that

$$\tilde{\chi}_k^0 = N_{k\ell} (\tilde{B}, \tilde{W}^3, \tilde{H}_d, \tilde{H}_u, \tilde{S}, \tilde{B}')_\ell, \quad (26)$$

where the physical neutralino states $\tilde{\chi}_k^0$ [$k = 1, \dots, 6$] are ordered according to ascending absolute mass values. The eigenvalues of the above matrix can be of both signs; the negative signs are incorporated to the mixing matrix N . Mathematically, this procedure of transforming a general complex symmetric matrix to the diagonal form with non-negative diagonal elements is called the Takagi diagonalization, or the singular value decomposition [18, 35]. Physically, the unitary matrix N determines the couplings of the mass-eigenstates $\tilde{\chi}_k^0$ to other particles.

Although the complexity of neutralino sector increases dramatically by this extension as compared to the MSSM (which can be solved analytically), the structure remains transparent since, in fact, the original MSSM and the new degrees of freedom are coupled weakly. M_K must be small by the requirement that the mixing of the $U(1)_X$ and $U(1)_Y$ sectors satisfy experimental limits. The remaining off-diagonal terms are suppressed with respect to the corresponding block diagonal terms by a factor of v/v_S . Since v_S sets the mass of the Z' , this results in v_S being roughly an order of magnitude greater than v . Therefore in physically interesting case of weak couplings of both the MSSM higgsino doublets to the singlet higgsino and to the $U(1)_X$ gaugino, and the coupling of the $U(1)_Y$ and $U(1)_X$ gaugino singlets, the remaining terms in the off-diagonal 4×2 submatrix in Eq. (25) are small. Then, an approximate analytical solution can be found following a two-step diagonalization procedure given in Ref. [18]. In the first step the 4×4 MSSM submatrix \mathcal{M}_4 and the new 2×2 singlino– $U(1)_X$ gaugino submatrix \mathcal{M}_2 are separately diagonalised. In the second step a block-diagonalization removes the non-zero off-diagonal blocks while leaving the diagonal blocks approximately diagonal up to second order, due to the weak coupling of the two subsystems.

2.4 The sfermion sector

As explained in the Introduction, we assume the exotic squarks to be substantially heavier than the MSSM fields. However the structure of the MSSM squarks gets modified by the presence of extra $U(1)_X$. Both the squarks and sleptons are important to our analysis and so we briefly describe the new ingredients in the sfermion mass matrix (neglecting the possibility of flavor and CP violation)

$$M_{\tilde{f}}^2 = \begin{pmatrix} m_{\tilde{F}}^2 + m_f^2 + \Delta_{\tilde{f}} & m_f(A_f - \mu(\tan\beta)^{-2I_f^3}) \\ m_f(A_f - \mu(\tan\beta)^{-2I_f^3}) & m_{\tilde{f}}^2 + m_f^2 + \Delta_{\tilde{f}^*} \end{pmatrix}. \quad (27)$$

where $m_{\tilde{F}}$, $m_{\tilde{f}}$ are the sfermion soft-supersymmetry breaking parameters for the quark and lepton doublets $F = Q, L$ and singlets $f = U^c, D^c, E^c$ and A_f is the trilinear coupling, while m_f is the corresponding fermion mass and the D -terms receive additional $U(1)_X$ terms

$$\Delta_{\tilde{f}} = M_Z^2 \cos 2\beta (I_f^3 - e_f s_W^2) + \frac{1}{2} g_1'^2 Q_{\tilde{f}} [v^2 (Q_1 \cos^2 \beta + Q_2 \sin^2 \beta) + Q_S v_S^2] \quad (28)$$

where I_f^3 and e_f are the weak isospin and electric charge and the $U(1)_X$ charges $Q_{\tilde{f}}$ are for the left fields. Explicitly, we have for squarks

$$\begin{aligned} \Delta_{\tilde{u}} &= M_Z^2 \cos 2\beta \left(\frac{1}{2} - \frac{2}{3} s_W^2\right) + \frac{1}{80} g_1'^2 [-v^2 (2 \sin^2 \beta + 3 \cos^2 \beta) + 5 v_S^2] \\ \Delta_{\tilde{u}^*} &= M_Z^2 \cos 2\beta \frac{2}{3} s_W^2 + \frac{1}{80} g_1'^2 [-v^2 (2 \sin^2 \beta + 3 \cos^2 \beta) + 5 v_S^2] \\ \Delta_{\tilde{d}} &= M_Z^2 \cos 2\beta \left(-\frac{1}{2} + \frac{1}{3} s_W^2\right) + \frac{1}{80} g_1'^2 [-v^2 (2 \sin^2 \beta + 3 \cos^2 \beta) + 5 v_S^2] \\ \Delta_{\tilde{d}^*} &= M_Z^2 \cos 2\beta \left(-\frac{1}{3} s_W^2\right) + \frac{2}{80} g_1'^2 [-v^2 (2 \sin^2 \beta + 3 \cos^2 \beta) + 5 v_S^2] \end{aligned} \quad (29)$$

and for sleptons

$$\begin{aligned} \Delta_{\tilde{\nu}} &= M_Z^2 \cos 2\beta \left(\frac{1}{2}\right) + \frac{2}{80} g_1'^2 [-v^2 (2 \sin^2 \beta + 3 \cos^2 \beta) + 5 v_S^2] \\ \Delta_{\tilde{e}} &= M_Z^2 \cos 2\beta \left(-\frac{1}{2} + s_W^2\right) + \frac{2}{80} g_1'^2 [-v^2 (2 \sin^2 \beta + 3 \cos^2 \beta) + 5 v_S^2] \\ \Delta_{\tilde{e}^*} &= M_Z^2 \cos 2\beta (-s_W^2) + \frac{1}{80} g_1'^2 [-v^2 (2 \sin^2 \beta + 3 \cos^2 \beta) + 5 v_S^2] \end{aligned} \quad (30)$$

Note that here g_1' is the GUT normalized $U(1)_X$ gauge coupling analogous to the GUT normalized hypercharge gauge coupling g_1 in the MSSM.

The diagonal form of the sfermion mass matrix is obtained, as usual, by a 2x2 rotation in the LR plane

$$M_{\tilde{f}}^{2\text{diag}} = U_{\tilde{f}}^T M_{\tilde{f}}^2 U_{\tilde{f}} \quad (31)$$

and the mass eigenstates are defined according to

$$\begin{pmatrix} \tilde{f}_1 \\ \tilde{f}_2 \end{pmatrix} = U_{\tilde{f}}^\dagger \begin{pmatrix} \tilde{f}_L \\ \tilde{f}_R \end{pmatrix} \quad (32)$$

with the convention that $m_{\tilde{f}_1} \leq m_{\tilde{f}_2}$.

3 Calculating the relic density

The calculation of the neutralino LSP relic density in the MSSM is well known [1, 2] and has been widely studied in the general MSSM [36] and the constrained MSSM [37]. The calculation of the relic density in the NMSSM has also been extensively studied [38]. The differences between the MSSM relic density calculation and the USSM calculation arise through the extension of the particle spectrum and through the new interactions that are introduced. We have implemented all new interactions into the `micrOMEGAs`[25] code using `LanHep`[24] to generate the feynman rules. `MicrOMEGAs` takes full account of all annihilation and coannihilation processes and calculates their effect whenever they are relevant. Nevertheless, from the form of these alterations we would like to make some general observations before we go on to consider the details of the calculations.

The USSM extends the neutralino sector by adding two new states to the spectrum: the bino' and singlino components. This results in two extra neutralinos. However for the relic density calculation we are only interested in the lightest neutralinos, so the primary effect will be through the magnitude of the singlino and bino' components in the lightest neutralino. In what follows we will be interested in the scenarios in which the lightest neutralino has a significant singlino component and a small but non-zero bino' component. Therefore it is informative to consider the general form of the interactions that arise from the singlino and bino' components of the lightest neutralino before considering specific diagrams.

The bino' component is always subdominant to the singlino component due to the see-saw structure of the extra 2×2 \tilde{S}/\tilde{B}' sector of the neutralino mass matrix in Eq. 25. The form of the interactions that arise from the inclusion of the bino' component closely mirror those of the bino component, except for the different coupling constant and charges under the new $U(1)_X$.

The singlino component is another matter. It gives rise to a new type of neutralino interaction from the $\lambda \hat{S} \hat{H}_u \hat{H}_d$ term in the superpotential that will be seen to dominate the annihilation processes of neutralinos with significant singlino components. This term means that if the lightest neutralino has significant singlino and higgsino components then it will couple strongly to Higgs bosons with a significant H_u or H_d component, usually the lighter Higgs bosons, $H_{1,2}$ and A in the spectrum. Moreover, the absence of the singlet cubic term \tilde{S}^3 , in contrast to the NMSSM, implies that the singlino-dominated LSP *needs* an admixture of MSSM higgsinos to annihilate to Higgs bosons.

On the other hand, the singlino component does not interact with the $SU(2)$ or $U(1)_Y$ gauginos. Therefore a significant singlino component in the lightest neutralino will suppress annihilations to W or Z_1 bosons.

Finally, there is no coupling of the singlino component to fermions. Thus a significant singlino component in the lightest neutralino will also suppress annihilation to fermions.

Having noted these general features we will now consider the specific behavior of the different annihilation diagrams.

3.1 t-channel diagrams

- Gauge boson final states

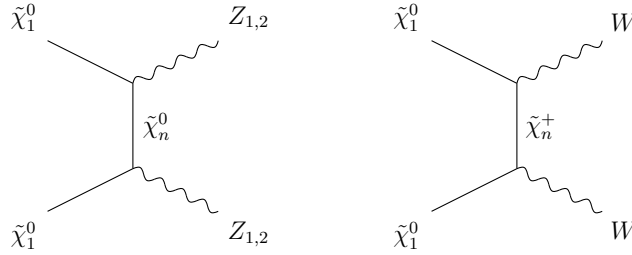


Figure 1: *The t-channel annihilation processes for a neutralino to final states containing gauge bosons.*

Fig. 1 shows the t-channel diagrams available for annihilation of neutralinos to gauge bosons. The $\tilde{\chi}_1^0 \tilde{\chi}_j^0 Z_i$ vertex is given in Eq. (B.1). Note that the coupling of neutralinos to the Z component of the Z_1 state is precisely that of the MSSM $\tilde{\chi}_1^0 \tilde{\chi}_j^0 Z$ coupling. As the Z component dominates the Z_1 state, a singlino dominated LSP will not annihilate strongly to Z_1 bosons.

In contrast there is a strong coupling from the MSSM-higgsino components as well as the singlino component to the Z' component of the Z_i state. Notice also that the MSSM-higgsino components of the LSP enter with the same sign in the coupling to the Z' , unlike in the coupling to the Z , where they tend to cancel each other. As the Z_2 boson is dominantly Z' any LSP with a non-zero higgsino or singlino fraction will annihilate to Z_2 bosons when such a final state is kinematically allowed. Unfortunately the Z_2 is required to be heavy by experimental limits, so annihilation of the lightest neutralinos to final states involving one Z_2 is hard to achieve and annihilation to two Z_2 bosons is impossible.

The second diagram of Fig. 1 shows the t-channel annihilation to W^\pm final states. Eqs. (B.2) and (B.3) give the relevant coupling and show that the singlino and bino' components do not couple to the wino component of charginos or to the W^\pm bosons. This means that a large singlino or bino' component in the LSP will suppress annihilation to W^\pm bosons in the final state.

- Higgs boson final states

Fig. 2 shows the available t-channel processes for the annihilation of neutralinos to final state Higgs bosons. Due to the $\lambda \hat{S} \hat{H}_u \hat{H}_d$ term in the superpotential and the D-terms there are significant differences between these diagrams in the USSM and the MSSM. The $\tilde{\chi}_1^0 \tilde{\chi}_i^0 H_j$ vertex given in Eq. (B.6) is the relevant vertex in this first diagram.

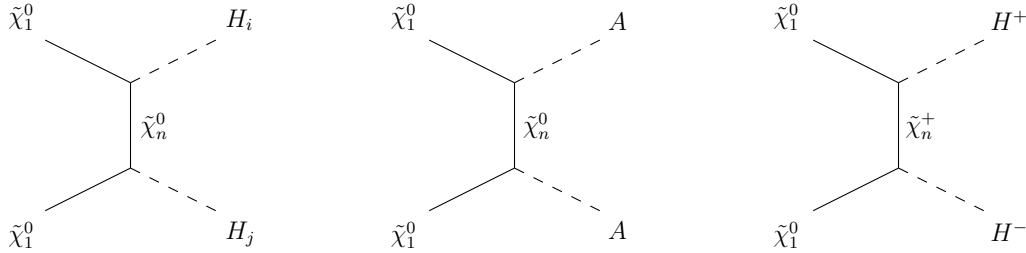


Figure 2: *The t-channel annihilation processes for a neutralino to final states involving scalar Higgs bosons, pseudoscalar Higgs bosons or charged Higgs bosons respectively.*

First note that the bino' component of one neutralino couples with the higgsino component of the other and the $H_{u,d}$ component of the final state Higgs boson in the same way as the equivalent coupling of the bino or wino components. In addition there is an extra term which couples the bino' component of one neutralino to the singlino component of the other and to the singlet component of the Higgs boson in the final state. This means that if the lightest neutralino is dominantly singlino, it will annihilate to final state Higgs bosons with a significant singlet component through the exchange of a neutralino with a significant bino' component in the t-channel. Unfortunately these processes are disfavored for the same reason as annihilation to final states containing a Z_2 . The Higgs boson with a significant singlet component will have a mass comparable to the Z_2 boson and thus a final state with two such Higgs bosons will be impossible and even one will often be kinematically ruled out.

Of more interest is the term in this vertex that couples a singlino component of one neutralino to a higgsino component of the other neutralino and the $H_{u,d}$ components of the Higgs boson with a strength λ . If the lightest neutralino is dominantly singlino then two LSPs can exchange a dominantly higgsino neutralino in the t-channel to produce two Higgs bosons in the final state. This is a channel that is always present if the lightest neutralinos are heavy enough to produce two light Higgs bosons in the final state. Obviously, if both H_1 and H_2 are lighter than the lightest neutralino then there will be more available channels. As the singlino couples predominantly to Higgs states, this channel provides the strongest annihilation mechanism for a neutralino with a large singlino component. This amplitude will be maximised for three degenerate mixed state neutralinos with strong higgsino and singlino components that are heavier in mass than the lightest two Higgs states. The addition of this vertex also allows for a new annihilation process for a dominantly higgsino neutralino through the exchange of a t-channel neutralino with a substantial singlino component.

The middle diagram of Fig. 2 shows the annihilation to final state pseudoscalar Higgs bosons. The relevant vertex is given in Eq. (B.10). The first line gives the familiar MSSM vertex for the coupling of a \tilde{B} or \tilde{W} component of a neutralino to a

higgsino component and a pseudoscalar Higgs. This is modified by an overall factor of $\cos \phi$ which determines the magnitude of the MSSM-like components of the pseudoscalar Higgs over the singlet contribution. As $\sin \phi \approx v \cos \beta / v_S$, the suppression from $\cos \phi$ is small. This is the same as saying that the pseudoscalar Higgs generally only has a very small singlet component. The analogue of the \tilde{W} , \tilde{B} interaction terms appears for the bino'. The bino' component also couples to the singlino component of the second neutralino and the singlet component of the final state pseudoscalar Higgs. This term is $\sin \phi$ suppressed due to the small singlet component of the A bosons in the final state. These interactions determine the strength of the annihilation of a dominantly gaugino LSP to pseudoscalar Higgs bosons through the exchange of a dominantly higgsino (or singlino) neutralino.

More interesting contributions come from the $\lambda \hat{S} \hat{H}_u \hat{H}_d$ term in the superpotential. These provide a $A \tilde{H}_u \tilde{H}_d$ coupling, albeit suppressed by a factor of $\sin \phi$. Such a coupling does not appear in the MSSM. There is also a term that couples $A \tilde{S} \tilde{H}_{u,d}$ with no $\sin \phi$ suppression. Once again this produces a strong annihilation channel for a neutralino with a substantial singlino component through t-channel neutralino exchange where the neutralino exchanged in the t-channel must have a significant higgsino component. This is the analogue of the process we discussed in some detail for the scalar Higgs final states and will, kinematics allowing, give a strong annihilation channel for a dominantly singlino neutralino as long as there is a light neutralino in the spectrum with a substantial higgsino component to be exchanged in the t-channel.

The final diagram of Fig. 2 shows annihilation to charged Higgs boson final states. The relevant vertex is given in Eq. (B.14). The vertex includes a \tilde{B}' interaction that parallels the familiar \tilde{B} and \tilde{W} interactions to the higgsino component of the chargino and a charged Higgs boson. There is also a term that arises from the $\lambda \hat{S} \hat{H}_u \hat{H}_d$ superpotential term. This allows for a neutralino with a substantial singlino component to annihilate to charged Higgs bosons via t-channel chargino exchange as long as there are light charginos with a significant higgsino component and the final state charged Higgs bosons are kinematically allowed. In contrast to the previous two diagrams, this one does not add an extra annihilation channel for a dominantly higgsino neutralino. In the first two diagrams there is the new possibility in which a dominantly singlino neutralino is exchanged in the t-channel. In the third diagram there is no such process as there is no singlino component in the charginos.

From an analysis of the processes with Higgs bosons in the final state we see that there will be a strong annihilation cross-section for a neutralino with a large singlino component to light Higgs bosons if there is a light neutralino with a substantial higgsino component in the spectrum and the Higgs boson final states are kinematically allowed. We also note that the $\lambda \hat{S} \hat{H}_u \hat{H}_d$ allows for new couplings between neutralinos and Higgs bosons that will alter the annihilation of dominantly higgsino neutralinos with respect to their behavior in the MSSM.

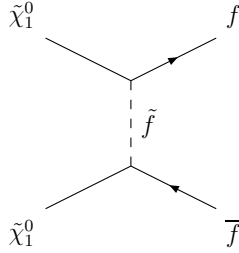


Figure 3: *The t-channel annihilation process for neutralinos to fermions.*

- Mixed boson final states

It is quite possible to have an unmatched pair of bosons in the final state of a t-channel annihilation diagram. We do not need to go through the details of all possible diagrams. Instead we just note that a neutralino with a significant singlino component will dominantly annihilate to final states made up of Higgs bosons. The strength of such channels will depend upon the size of the singlino component in the lightest neutralino, the mass of the neutralinos with substantial higgsino components that will be exchanged in the t-channel, and the mass of the final state Higgs bosons.

- Fermion final states

Finally we consider the t-channel annihilation diagram to final state fermions through the diagram given in Fig. 3. The squark vertices are given in Eqs. (B.18) and (B.19). The couplings of the bino and wino components of the neutralino are the same as in the MSSM. Note that there is an extra coupling of the bino' component of the neutralino to the squark-quark pair that is of the same order of magnitude as for the \tilde{B} . As the bino' is only ever a subdominant component of the lightest neutralino, and as the annihilation to fermions is relatively weak in the first place, we can expect that interactions of this form will have little impact on the annihilation cross-section. However, if the lightest neutralino is too light to annihilate to final state Higgs bosons, this channel will remain open and can dominate though it will give a relic density well in excess of that measured by WMAP.

3.2 s-channel diagrams

Fig. 4 shows the possible s-channel processes available for the annihilation of a pair of neutralinos. The first diagram shows the annihilation through and intermediate Z_i gauge boson. The relevant coupling of two neutralinos to a Z_i is given in Eq. (B.1). As before we note that the singlino component of the neutralino only couples to the Z' component of the Z_i gauge boson. This means that if the lightest neutralino has

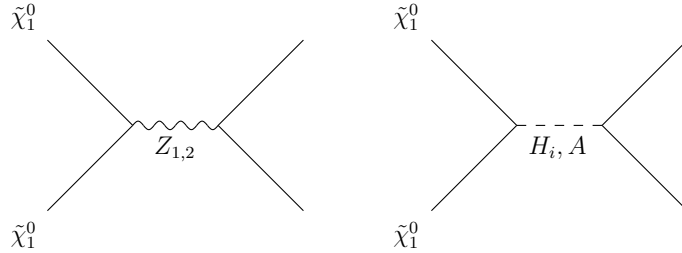


Figure 4: *The annihilation processes for a neutralino through s-channel Higgs and Z_i bosons, where we do not specify the precise particles in the final state.*

a significant singlino component, then annihilations through an s-channel Z_1 will be suppressed as the Z' component of the Z_1 is required to be very small. On the other hand, the Z_2 has a large Z' component. Therefore a lightest neutralino with a substantial singlino component will annihilate through an s-channel Z_2 .

The second diagram shows the annihilation of neutralinos through an s-channel scalar or pseudoscalar Higgs boson. The relevant couplings are given in Eq. (B.6) and Eq. (B.10) respectively. Consider first the case in which the s-channel Higgs boson is dominantly composed of the singlet Higgs. Since the bino or wino components of the lightest neutralino only couple to the non-singlet Higgs components of the s-channel Higgs a light neutralino that is dominantly wino or bino will not annihilate strongly through a dominantly singlet Higgs. However there is a coupling of the singlet component of the Higgs boson to the higgsino components of the lightest neutralino. This provides a strong channel when on-resonance for annihilation of a light neutralino with a large higgsino component. There is also a strong coupling if the lightest neutralino has significant bino' and singlino components. Thus we expect a light neutralino with strong mixing between higgsino, singlino and bino' terms to annihilate strongly through s-channel heavy Higgs exchange where the heavy higgs has a large singlet Higgs component.

If the s-channel Higgs boson does not have a large singlet Higgs component then the story is somewhat different. In this case the light neutralino needs to have a significant higgsino fraction along with a substantial contribution from one of the other non-higgsino states. This situation is mirrored in the case of the pseudoscalar Higgs.

From this we see that we have a new annihilation channel for neutralinos with a significant higgsino fraction through a dominantly singlet Higgs in the s-channel. We also see that a light neutralino with a substantial singlino-higgsino mixture will annihilate strongly through the whole range of s-channel Higgs exchange processes.

3.3 Coannihilation

As well as the annihilation of two identical neutralinos, it is often the case that coannihilation between the LSP and the NLSP (and sometimes even heavier states) can be important. This process is normally important for a dominantly MSSM-higgsino or wino neutralino LSP. In these situations there is an automatic near degeneracy in the mass of the lightest neutralino with the mass of the lightest chargino and, in the case of the higgsinos, also with the next-to-lightest neutralino. A dominantly singlino LSP does not have an automatic degeneracy with other states. However, it is possible for a singlino neutralino to be exactly degenerate with other states - something that does not happen in the MSSM due to the signs of the terms in the neutralino mixing matrix. In these cases we would expect the effect of coannihilation to be important.

Therefore we expect coannihilation processes to only be significant in regions of the parameter space where we move from one type of LSP to another as this indicates a degeneracy in the mass of the LSP and NLSP. We also expect to see the standard large coannihilation contributions for a predominantly MSSM-like higgsino LSP or predominantly wino LSP.

4 Elastic scattering of neutralinos from nuclei

The direct cold dark matter search experiments, such as DAMA/LIBRA, CDMS, ZEPLIN, EDELWEISS, CRESST, XENON, WARP [39], aim at detecting dark matter particles through their elastic scattering with nuclei. This is complementary to indirect detection efforts, such as GLAST, EGRET, H.E.S.S. [40], which attempt to observe the annihilation products of dark matter particles trapped in celestial bodies.

Since we assume the LSP to be the lightest neutralino $\tilde{\chi}_1^0$, we consider the elastic scattering of the lightest neutralino from nuclei. The elastic scattering is mediated by the t -channel Z_i and Higgs H_k exchange, as well as the s -channel squark \tilde{q}_j exchange, as depicted in Fig.5 for $\tilde{\chi}_1^0 q$ scattering. There are also important contributions from interactions of neutralinos with gluons at one loop [42, 43].

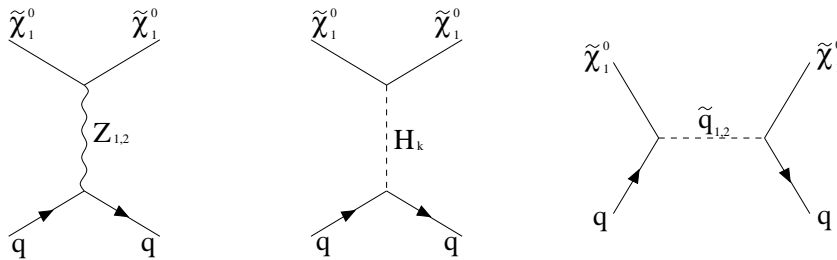


Figure 5: *Diagrams contributing to the lightest neutralino scattering from a quark.*

The extended particle content and new couplings present in the USSM model have also a direct effect on the elastic cross section calculations, as discussed in the previous chapter.

The elastic cross section for neutralino scattering from a nucleus can be broken into a spin-independent (SI) and a spin-dependent (SD) part,

$$\sigma = \sigma_{\text{SI}} + \sigma_{\text{SD}}, \quad (33)$$

each of which can be expressed in terms of the elastic scattering of neutralino from individual nucleons in the nuclei. In the limit of zero-momentum transfer they can be written as [41]

$$\sigma_{\text{SI}} = \frac{4m_r^2}{\pi} [Zf_p + (A - Z)f_n]^2, \quad (34)$$

$$\sigma_{\text{SD}} = \frac{32m_r^2}{\pi} G_F^2 J(J + 1) \Lambda^2, \quad (35)$$

where Z and A are atomic number and mass of the nucleus, J is the total nucleus angular momentum and m_r is the reduced neutralino-nucleus mass. Note that the spin-independent part benefits from coherent effect of the scalar couplings, which leads to cross section and rates proportional to the square of the atomic mass of the target nuclei.

The spin-dependent quantity Λ is given by

$$\Lambda_n = \frac{1}{J} \left[\langle S_p \rangle \sum_{q=u,d,s} \frac{A_q}{\sqrt{2}G_F} \Delta_q^p + \langle S_n \rangle \sum_{q=u,d,s} \frac{A_q}{\sqrt{2}G_F} \Delta_q^n \right] \quad (36)$$

where $\langle S_p \rangle$ and $\langle S_n \rangle$ are the expectation values of the spin content of the proton and neutron group in the nucleus, while Δ_q^p and Δ_q^n are the quark spin content of the proton and neutron, respectively.

For the spin-independent part, the effective couplings of the LSP neutralino to proton and neutron f_p and f_n are more complicated. In the limit of $m_{\tilde{\chi}_1^0} \ll m_{\tilde{q}}$ and $m_q \ll m_{\tilde{q}}$, which we will later confine to, they simplify and can be approximated as:

$$\frac{f_{p,n}}{m_{p,n}} = \sum_{q=u,d,s} f_{T_q}^{p,n} \frac{B_q}{m_q} + \frac{2}{27} f_{T_G}^{p,n} \sum_{q=c,b,t} \frac{B_q}{m_q} \quad (37)$$

The first term in Eq.(37) corresponds to interactions with the quarks in the target nuclei, while the second term corresponds to interactions with the gluons in the target through a quark/squark loop diagram, and

$$f_{T_G}^{p,n} = 1 - \sum_{q=u,d,s} f_{T_q}^{p,n}. \quad (38)$$

Finally, the effective Lagrangian for elastic scattering of neutralinos from quarks in the non-relativistic limit can be written as a sum of axial-vector (spin-dependent) and scalar (spin-independent) terms:

$$\mathcal{L}_{\text{eff}} = A_q (\bar{\chi}_1 \gamma^\mu \gamma_5 \chi_1) (\bar{q} \gamma_\mu \gamma_5 q) + B_q (\bar{\chi}_1 \chi_1) (\bar{q} q) \quad (39)$$

The effective couplings A_q and B_q are given by:

$$A_q = \frac{g_2^2}{16} \sum_{i=1,2} \frac{|B_q^{iL}|^2 + |B_q^{iR}|^2}{m_{\tilde{q}_i}^2 - (m_{\tilde{\chi}_0} - m_q)^2} - \frac{G_F}{\sqrt{2}} [|N_{13}|^2 - |N_{14}|^2] I_q^3 \\ - \frac{g_1'^2}{4m_{Z'}^2} [Q_1 |N_{13}|^2 + Q_2 |N_{14}|^2 + Q_s |N_{15}|^2] (Q_Q + Q_{\bar{q}}) \quad (40)$$

$$B_q = -\frac{g_2^2}{8} \sum_{i=1,2} \frac{\text{Re}(B_q^{iL} B_q^{iR*})}{m_{\tilde{q}_i}^2 - (m_{\tilde{\chi}_0} - m_q)^2} \\ - \frac{h_q}{2\sqrt{2}} \sum_{k=1}^3 \frac{\text{Re}(G_k) + \text{Re}(G'_k) + \text{Re}(G''_k)}{m_{H_k}^2} \begin{cases} \mathcal{O}'_{1k} & \text{for } q = d, s, b \\ \mathcal{O}'_{2k} & \text{for } q = u, c, t \end{cases} \quad (41)$$

In this expressions we have neglected a small Z - Z' mixing.

The first terms in both effective couplings come from squark exchange diagrams. The neutralino-squark-quark couplings B_q^{iL} , B_q^{iR} are given in Appendix B. As seen in Eqs. (B.20,B.21), they receive a contribution from the bino' component N_{16} .

The second and the third terms in (40) come from the Z and Z' exchanges, respectively, where the latter contains a term due to the singlino component, N_{15} . The second term in the form factor B_q receives contributions from three scalar Higgs boson exchanges. Each contains an MSSM-like term, G_k , as well as the new terms G'_k and G''_k , ($k = 1, 2, 3$)

$$G_k = g_2 (N_{12} - t_W N_{11}) (N_{14} \mathcal{O}'_{2k} - N_{13} \mathcal{O}'_{1k}) \\ G'_k = -2 g_1' N_{16} (Q_1 N_{13} \mathcal{O}'_{1k} + Q_2 N_{14} \mathcal{O}'_{2k} + Q_s N_{15} \mathcal{O}'_{3k}) \\ G''_k = \sqrt{2} \lambda [N_{15} (N_{13} \mathcal{O}'_{2k} + N_{14} \mathcal{O}'_{1k}) + N_{13} N_{14} \mathcal{O}'_{3k}] \quad (42)$$

The G'_k piece is generated by the $g_1' \tilde{B}'(\tilde{H}_i H_i + \tilde{S} S)$ couplings from the extra $U(1)_X$ D -terms, while the G''_k is induced by the $\lambda \tilde{H}_i(\tilde{S} H_j + \tilde{H}_j S)$ couplings (here we follow the conventions and notations of Ref. [44], properly extended to the USSM model [45]).

5 Results

Now that we have introduced the model we move on to study the details of the dark matter phenomenology within the USSM parameter space.

5.1 Defining a parameter range

Before we study the phenomenology we need to define the parameter range we are interested in. The USSM extends the number of free parameters over those in the MSSM by the set:

$$M'_1, g'_1, \lambda, A_\lambda, v_S.$$

These parameters are constrained by a number of different factors.

We fix $g'_1 = g_1$ as we wish to maintain gauge coupling unification and the two $U(1)$ gauge couplings run with identical RGEs.

The parameters v_S , λ , A_λ appear in the determination of particle masses. Therefore we determine these by setting the corresponding masses. First of all, we wish to keep v_S low to maximise the region of parameter space in which there is a light singlino/bino' LSP. If $M'_1 = 0$ then there are two degenerate singlino/bino' neutralinos with a mass $Q'_S g'_1 v_S$. However, we do not have the freedom to set v_S arbitrarily low since from Eqs. (9) we see that low v_S would require a light Z_2 mass and a large Z - Z' mixing incompatible with the LEP and Tevatron limits. Adopting

$$m_s = g'_1 v_S = 1200 \text{ GeV}, \tag{43}$$

together with assumed $\tan \beta = 5$, gives $M_{Z_2} = 949 \text{ GeV}$ and $\sin_{ZZ'} = 3 \cdot 10^{-3}$ which is consistent with current constraints. We use this to set the magnitude of the v_S in all that follows.

With v_S set, our choice of λ will set the size of μ through the relation

$$\mu = \lambda \frac{v_S}{\sqrt{2}}. \tag{44}$$

Note that λ is a coupling and so cannot be too large. An upper limit on $\lambda < 0.7$ at a given value of v_S results in a corresponding maximum value on μ , and consequently $\mu < m_{S,Z'}$. As a result, $m_{\tilde{\chi}_1^0} < m_{Z',S}$ will always be satisfied which has important implications for the available dark matter annihilation channels. It also justifies our earlier claim that there will always be light charginos and higgsinos in the spectrum if the Z' mass is low.

We set the size of A_λ by setting the mass of the pseudoscalar Higgs. From Eq. (20) we see that once the VeV of S and λ have been set, the mass of m_A only depends upon $\tan \beta$ and A_λ . As we are keeping $\tan \beta$ fixed, we can use A_λ to set the pseudoscalar Higgs mass.

The familiar MSSM parameters are also relevant to the details of both the relic density calculation and the direct detection phenomenology. The most important parameters are those that appear in the neutralino mass matrix - M_1 and M_2 . We keep the ratio $M_1 : M_2 = 1 : 2$ for simplicity, but there are as many ways to break this relation in the USSM as in the MSSM.

Finally we must set M'_1 . In what follows we take M'_1 as a free variable and scan over a range of values. In our first study we take M'_1 to be independent of the other gaugino masses, as in the study of Ref. [18] where the collider phenomenology has been discussed. This will complement Ref. [18] with the dark matter calculations. On the other hand, it is also interesting to consider a scenario in which soft SUSY breaking gaugino masses are unified, namely $M_1 : M'_1 : M_2 = 1 : 1 : 2$ and we do this in our second scenario. This allows us to organize our studies in the following way:

- scenario A: M'_1 arbitrary ;
- scenario B: unified gaugino masses $M'_1 = M_1 = M_2/2$.

To calculate the relic density we need to set the rest of the particle spectrum. To do this we fix the pseudoscalar Higgs mass $m_A = 500$ GeV and for sfermion masses we take a common mass of $m_{Q,u,d,L,e} = 800$ GeV, and a common trilinear coupling $A = 1$ TeV, while the gluino mass is determined assuming unified gaugino masses at the GUT scale. We have set the squarks and sleptons to be heavy as this allows for a clearer analysis of the annihilation properties of the neutralinos.

For the direct dark matter searches, there are large uncertainties in the spin-dependent and spin-independent elastic cross section calculations due to the poor knowledge of the quark spin content of the nucleon and quark masses and hadronic matrix elements. These uncertainties have recently been discussed in Ref. [46], from where we calculate the central values of $f_{Tq}^{p,n}$:

$$\begin{aligned} f_{T_u}^p &= 0.027, & f_{T_d}^p &= 0.039, & f_{T_s}^p &= 0.36 \\ f_{T_u}^n &= 0.0216, & f_{T_d}^n &= 0.049, & f_{T_s}^n &= 0.36 \end{aligned} \quad (45)$$

and $\Delta_q^{p,n}$:

$$\begin{aligned} \Delta_u^p &= +0.84, & \Delta_d^p &= -0.43, & \Delta_s^p &= -0.09 \\ \Delta_u^n &= -0.43, & \Delta_d^n &= +0.84, & \Delta_s^n &= -0.09 \end{aligned} \quad (46)$$

5.2 Scenario A: M'_1 arbitrary

In this scenario we take M'_1 as an arbitrary parameter with the MSSM gaugino parameters fixed at $\mu = 300$ GeV, $M_1 = M_2/2 = 750$ GeV.

5.2.1 Mass spectrum

With these parameters we calculate the resulting mass spectrum at a given value of M'_1 . The mass spectrum for $M'_1 = 0$ GeV is shown in Fig. 6. In the Higgs sector we have a light Higgs at 127 GeV, a heavier scalar, pseudoscalar and charged Higgses around 500 GeV and a dominantly singlet Higgs at 949 GeV. Sfermions are located between 750

Parameter	Value
M_1	750 GeV
M_2	1500 GeV
μ	300 GeV
M'_1	0-20 TeV
$\langle S \rangle$	2607.61 GeV
λ	0.163
A_λ	160 GeV

Table 2: The parameters taken for the neutralino sector in the scan with $\mu = 300$ GeV, $m_A = 500$ GeV, $\tan\beta = 5$.

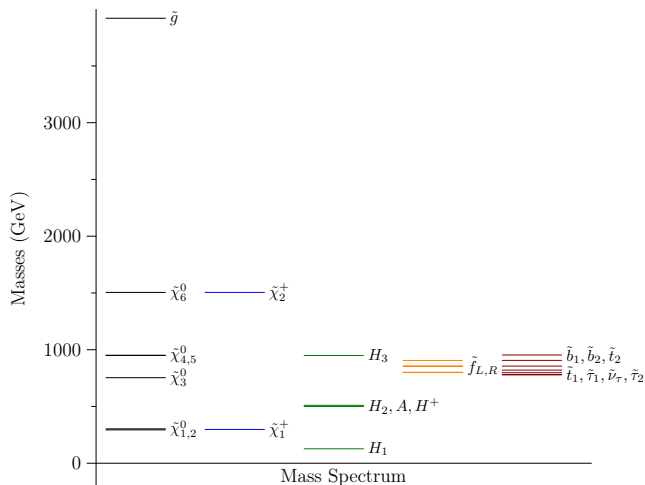


Figure 6: The mass spectrum for $M'_1 = 0$ GeV

to 950 GeV. The chargino sector consists of a higgsino-like chargino around 300 GeV and a wino-like chargino at 1500 GeV. Since the mixing between the MSSM-like and the bino'/singlino at $M'_1 = 0$ GeV is numerically small, the spectrum of neutralinos can qualitatively be understood by separately diagonalizing the 4x4 and 2x2 neutralino mass sub-matrices. Thus to a good approximation we have (according to ascending (absolute) masses for $M'_1 = 0$ GeV) a pair of nearly degenerate, maximally mixed MSSM higgsinos at 300 GeV (first two states), an MSSM bino at 750 GeV (the third), a pair of nearly degenerate, maximally mixed singlino/bino' neutralinos at 949 GeV (the fourth and the fifth) and an MSSM wino at 1500 GeV (the sixth state).

To understand the change of neutralino masses and of their composition as a function of M'_1 it is instructive to follow their analytic evolution as M'_1 is turned on. The see-saw

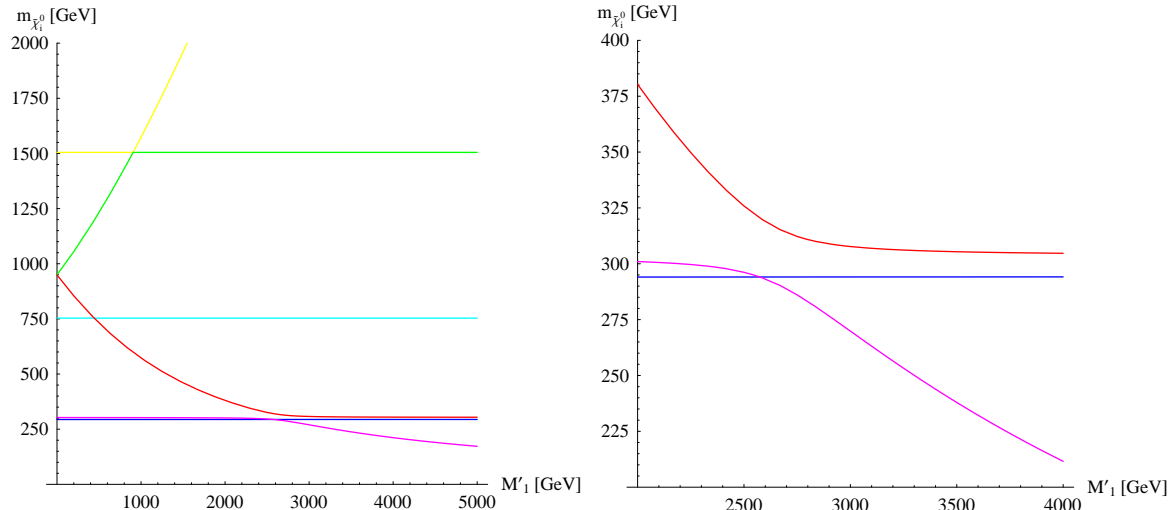


Figure 7: *The neutralino mass spectrum for varying M'_1 , for the parameter choices in table. 2. The right panel is a magnified part of the left one.*

structure of the 2x2 singlino/bino' submatrix forces the two nearly degenerate, mixed singlino/bino' states to move apart: the lighter one (the fourth) gets lighter, and the mass of the other (the fifth one) heavier as M'_1 increases. The MSSM-like states do not evolve much, unless the mass of one of the new states comes close to one of the MSSM, where a strong mixing may occur. For the mixing to be important not only the (absolute) masses must come close, but also the mass-eigenstates must belong to eigenvalues of the same sign. It is obvious from the see-saw structure that the heavier singlino/bino' state (the fifth one) belongs to the positive and the lighter (the fourth) to the one negative eigenvalue. Similarly the lighter of the two nearly degenerate MSSM higgsinos (the first state) belongs to the positive, and the other (the second) to negative eigenvalue.

As M'_1 increases the (absolute) mass of the fourth state gets closer to the third, however they do not mix since they belong to eigenvalues of opposite sign. In left panel of Fig. 7 the lines representing these two states pass each other at $M'_1 \sim 450$ GeV. The bino, which is the third state according to the mass ordering below 450 GeV, becomes the fourth one when M'_1 passes 450 GeV. On the other hand when M'_1 approaches 900 GeV and the mass of the fifth state gets close to the sixth one, strong mixing occurs between these states – the two lines representing these states in Fig. 7 "repel" each other. The heaviest neutralino smoothly changes its character from the MSSM wino to the singlino/bino' when M'_1 passes the cross-over zone near 900 GeV. Even more

interesting feature occurs when M'_1 approaches 2500 GeV, as illustrated in the right panel of Fig. 7 – a magnified part of the left panel. The singlino/bino' state belonging to the negative eigenvalue (which is now the third state according to mass ordering) mixes strongly with the second one. It does not mix with the first one since these states belong to eigenvalues of opposite sign. As a result of the mixing the mass of the second state is pushed down and below the lightest one for M'_1 above ~ 2.6 TeV. Thus the LSP discontinuously changes its character from being mainly higgsino to mainly singlino/bino' when M'_1 passes the cross-over zone near 2.6 TeV. For higher M'_1 values the LSP becomes dominantly singlino. This behavior will be important to understand discontinuities in plots to follow.

5.2.2 Relic density

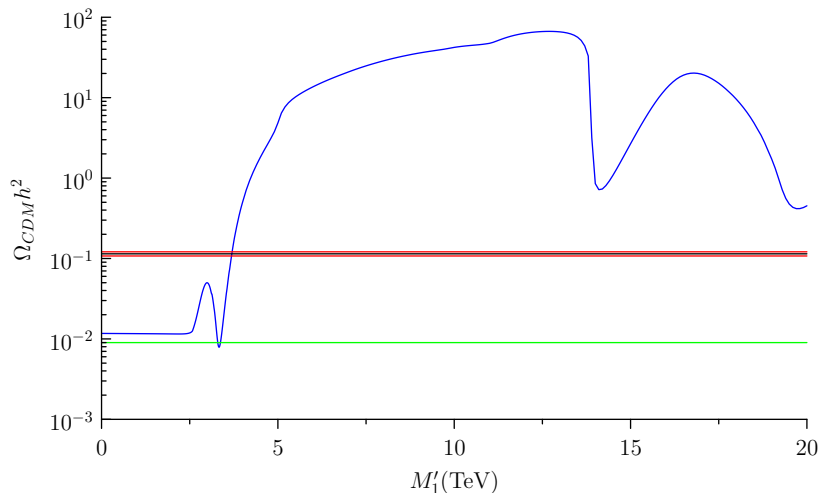


Figure 8: *The relic density across varying M'_1 , for $\mu = 300$ GeV, $m_A = 500$ GeV and $\tan\beta = 5$. The red lines show the 2σ measurement of the $\Omega_{CDM}h^2$ by WMAP-5. The green line shows the approximate MSSM higgsino relic density for $\mu = 300$ GeV.*

Having set the masses, we vary M'_1 and calculate the relic density. The resulting values for the relic density are plotted in Fig. 8. Before dealing with the specific channels that give rise to the different features, we make some general points. Firstly, as $\mu = 300$ GeV and $m_{A,H,H^\pm} \approx 500$ GeV it is never possible for a pair of neutralinos to annihilate to a pair of pseudoscalar Higgs bosons, medium mass Higgs bosons or charged Higgs bosons in the final state. Secondly, as the squarks and sleptons are significantly more massive than the mass of the LSP, they do not contribute significantly to the annihilation cross-section except where noted below.

In the range $0 < M'_1 < 2.5$ TeV the LSP is predominantly composed of MSSM-higgsino and gives a relic density of the same order of magnitude as an MSSM-higgsino. At $M'_1 = 2.57$ TeV the LSP becomes dominantly singlino, as shown by the cross-over of the mass lines in Fig. 7. As M'_1 increases, the singlino component of the LSP increases steadily. This decreases the strength of the $\tilde{\chi}_1^0 - \tilde{\chi}_1^\pm$ coannihilation that dominates the annihilation amplitude for a predominantly MSSM-higgsino LSP. As a result we might expect the value of $\Omega_{CDM}h^2$ to increase noticeably before $M'_1 = 2.57$ TeV. However, as M'_1 approaches 2.57 TeV the mass splitting between $\tilde{\chi}_1^0$ and $\tilde{\chi}_2^0$ decreases. This increases the amplitude for $\tilde{\chi}_1^0 - \tilde{\chi}_2^0$ coannihilation. This increase compensates the drop in the neutralino-chargino coannihilation and results in an almost flat value of $\Omega_{CDM}h^2$ up to $M'_1 = 2.57$ TeV.

Above $M'_1 = 2.57$ TeV the mass splitting between the lightest neutralino and the lightest chargino and next to lightest neutralino increases steadily. This quickly turns off any coannihilation processes. At the same time, the singlino component of the lightest neutralino increases quickly. This steadily reduces the amplitude of $\tilde{\chi}_1^0 - \tilde{\chi}_1^\pm$ annihilations. As a result of the combination of these two effects there is a sharp rise in the relic density above $M'_1 = 2.57$ TeV.

At $M'_1 \approx 3$ TeV we see a sharp dip in the value of $\Omega_{CDM}h^2$ caused by the pseudoscalar Higgs s-channel resonance. Just below $M'_1 = 5$ TeV we see a sharp jump in the relic density as the LSP drops below the top mass, ruling out processes of the form $\tilde{\chi}_1^0 \tilde{\chi}_1^0 \rightarrow H^* \rightarrow t\bar{t}$. By $M'_1 = 5$ TeV the LSP is 94% singlino with a 3% bino' admixture and a 2% higgsino admixture. This, combined with the mass splitting between the higgsinos and the singlino LSP, suppresses the annihilation of the singlino resulting in a relic density well above the measured value. At this point the dominant annihilation channel is to b, \bar{b} through off-shell s-channel Higgs production, with a subdominant contribution from t-channel higgsino exchange to final state light Higgs bosons. A small kink in the relic density profile at $M'_1 \approx 11$ TeV is the point at which the singlino becomes lighter than the light Higgs boson and final states with two Higgs bosons become kinematically disallowed. The dip at $M'_1 = 14$ TeV is the light Higgs resonance and the dip at $M'_1 = 20$ TeV is the Z_1 resonance.

Here we have seen that the dominant annihilation channels of the singlino - through t-channel higgsino exchange and through s-channel Higgs production - are not strong enough to give a relic density in agreement with the measured value. The exception is when the singlino is mixed with a higgsino state. This enhances the annihilation through s-channel Higgs production as the neutralino-neutralino-Higgs vertices require a non-zero higgsino contribution. It also enhances annihilation through t-channel higgsino exchange as the higgsinos are lighter.

The fact that we find a large relic density for a singlino LSP is partly down to our choice of parameters. Singlino dark matter dominantly annihilates to Higgs bosons, and with the parameters chosen above all but the lightest Higgs boson are excluded from the final state by kinematics and s-channel processes are similarly suppressed by the

large masses. This would not be the case if we were to take $m_{A,H,H^\pm} < \mu$. We can do this by either lowering A_λ or increasing λ . Raising λ also has the effect of increasing the coupling strength of the relevant vertices for singlino annihilation. We will discuss these effects further in scenario B.

5.2.3 Direct detection

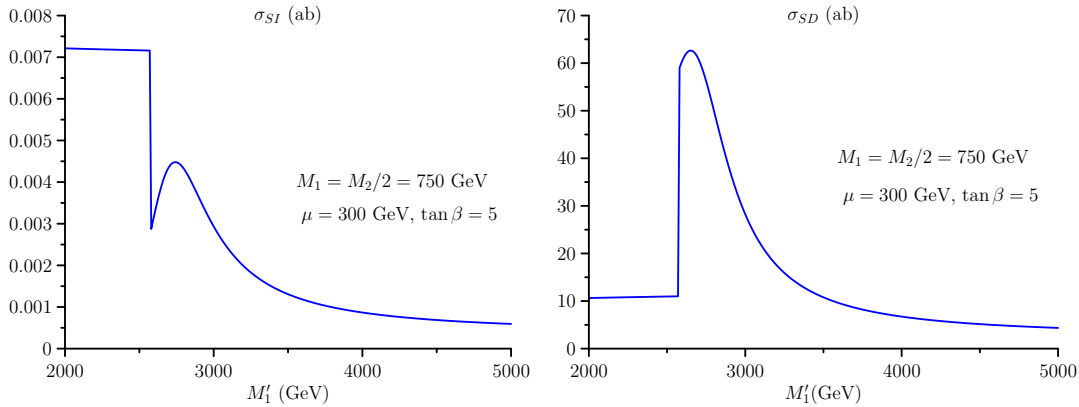


Figure 9: *The elastic spin-independent (left) and spin-dependent (right) LSP-proton cross section as a function of M'_1 in scenario A.*

Let us now turn to the direct DM detection analysis. In Fig. 9 the spin-independent as well as spin-dependent elastic cross section of the lightest neutralino on a proton is shown as a function of M'_1 . We restrict the range of M'_1 to 2–5 TeV, since beyond this range the cross section changes monotonically.

To understand the M'_1 behavior, we refer to Fig.7. Up to $M'_1 \sim 2.5$ TeV the lightest neutralino is almost a pure MSSM higgsino. As a result its couplings do not depend on M'_1 and the scattering cross sections are practically determined by the MSSM-like terms G_k . Both the SI and SD cross sections are almost equal to the MSSM result with corresponding parameters.

The discontinuity in the cross sections around 2.5 TeV is related to the sudden change of the nature of the LSP. As the M'_1 parameter increases, the mixing between the third and the second states pushes the latter below the lightest one (right panel of Fig.7). The nature of the LSP therefore changes discontinuously from one of the MSSM-like higgsinos to the other higgsino state which at the same time acquires an increasing singlino component.

The reduction of the spin-independent cross section (left panel) can be understood by realizing that the elastic cross section of the second-lightest state (according to mass ordering below $M'_1 = 2.5$ TeV) on the proton is more than an order of magnitude smaller

than that for the lightest one. When it becomes the LSP (for $M'_1 > 2.5$ TeV) the SI cross section drops significantly. As the singlino component of the LSP increases with M'_1 the G''_k factors, which are sensitive to both the singlino and the higgsino components – viz. Eq. (42), become responsible for the rise of the cross section. With further increase of M'_1 the LSP becomes almost a pure singlino which explains a steady fall of the cross section.

The spin-dependent cross section is dominated by the gauge boson exchange diagram. The Z coupling to the lightest neutralino is controlled by the combination $c_{34} \equiv |N_{13}|^2 - |N_{14}|^2$ of neutralino mixing matrix elements. For low M'_1 the lightest neutralino is almost a perfect mixture of \tilde{H}_d^0 and \tilde{H}_u^0 for which these elements almost entirely cancel resulting in a small value of c_{34} . As M'_1 increases the singlino forces the second-lightest state to become the lightest (flipping the sign of the coupling) and upsets this delicate cancelation. As a result, the cross section increases by a factor 6 and then starts to fall as the LSP becomes dominantly a pure singlino state.

5.3 Scenario B: $M_1 = M'_1 = M_2/2$

In the previous subsection we have considered the phenomenology of the USSM with non-universal M_1 and M'_1 . In this section we will consider the scenario in which gaugino masses are unified at the GUT scale implying the ratio $M_1 : M'_1 : M_2 = 1 : 1 : 2$ at the electroweak scale. We will vary M'_1 (together with other gaugino masses) as before and consider the behavior of both the relic density and the direct detection behavior. Motivated by the remarks at the end of Subsection 5.2.2 we also increase the value of μ parameter by a factor of 2, i.e. we take $\mu = 600$ GeV. This is achieved by doubling the size of λ .

5.3.1 Mass spectrum

Again to understand qualitatively the neutralino mixing pattern we start the discussion with $M'_1 = 0$. After the Takagi diagonalization of the neutralino mass matrix at $M'_1 = 0$ we find two almost massless eigenstates (dominated by the MSSM bino and wino components), a pair of nearly degenerate, maximally mixed MSSM higgsinos at ~ 600 GeV (the third and fourth states) and a pair of nearly degenerate, maximally mixed singlino/bino' neutralinos at 949 GeV (the fifth and sixth). The LEP limit on the lightest chargino mass therefore enforces $M'_1 \gtrsim 55$ GeV.

For understanding the neutralino mixing pattern as a function of M'_1 it is important to remember that the lighter of the two singlino/bino' and the lighter of the two higgsino states belong to negative eigenvalues, while the other states to positive eigenvalues. When the M'_1 parameter is switched on, the mixing pattern is more rich since not only the singlino/bino', but also the bino and wino states vary considerably, see Fig. 10. As a result there are more cross-over zones where mixing is important. In the cross-over

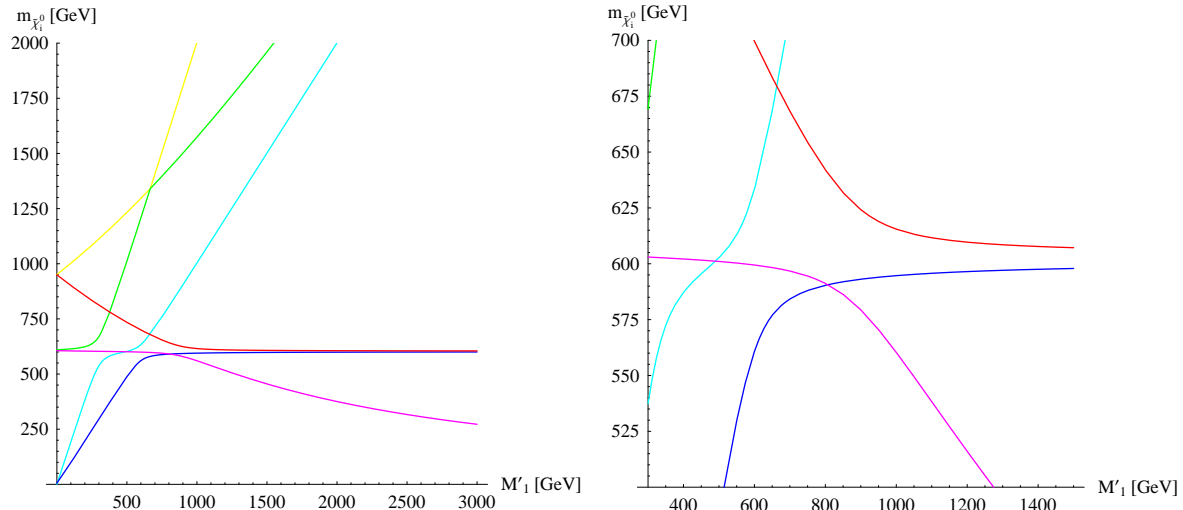


Figure 10: *The neutralino mass spectrum as a function of M'_1 in the unified scenario $M'_1 = M_1$. The effective μ parameter is set to 600 GeV, other parameters as in the previous subsection. Right panel is a magnified part of the left one.*

zone around $M'_1 \sim 270$ GeV the wino mixes with the heavier higgsino, around 500 GeV the bino mixes with the heavier higgsino, around 550 GeV the wino mixes with the heavier singlino/bino' and in the last zone around 900 GeV the lighter higgsino mixes with the lighter singlino/bino' state. This is illustrated in Fig. 10. As the lines develop from $M'_1 = 0$ GeV, the dominant component of the corresponding state changes its nature. For example, along the green line the state starts at $M'_1 = 0$ GeV as a heavier higgsino, then gradually becomes a wino-dominated (for $M'_1 \sim 400 - 600$ GeV) and finally (for $M'_1 > 600$ GeV) a bino'-dominated neutralino. The LSP mass, as we increase M'_1 , first increases, then levels off at $M_{LSP} \approx 600$ GeV and then decreases along with M'_1 . Its nature also changes. It starts as a bino, at $M'_1 \sim 600$ GeV gradually changes to a higgsino-dominated state and at $M'_1 \sim 800$ GeV discontinuously jumps to a singlino/bino'-dominated state. For higher values of M'_1 the lightest neutralino becomes mostly singlino.

5.3.2 Relic density

In Fig (11) we show the relic density calculation for coupled gaugino masses and $\mu = 600$ GeV. In this case the relic density phenomenology is significantly more complex than previously. First of all, note that below $M'_1 = 0.75$ TeV the LSP is predominantly bino, with non-zero admixtures from all other states. Above $M'_1 = 0.75$ TeV the LSP

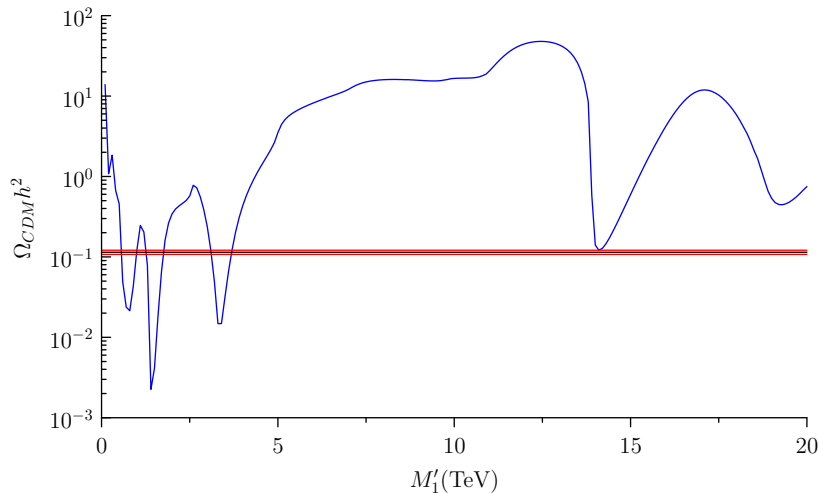


Figure 11: *The relic density across varying M'_1 with $M'_1 = M_1 = M_2/2$, for $\mu = 600$ GeV, $m_A = 500$ GeV and $\tan\beta = 5$.*

is predominantly singlino with substantial admixtures of bino' and higgsino. Around $M'_1 = 0.75$ TeV the LSP is predominantly higgsino with a large admixture of both singlino and bino.

If we initially ignore the resonances we can see a general trend in the relic density from a large value at low M'_1 , down to a lower value at around $M'_1 = 0.75$ TeV and then back to larger values at high M'_1 . This is to be expected as this follows the evolution of the LSP from bino (that generally gives $\Omega_{CDM}h^2 \gg \Omega_{WMAP}$) through higgsino (generally $\Omega_{CDM}h^2 \ll \Omega_{WMAP}$) to singlino ($\Omega_{CDM}h^2 \gg \Omega_{WMAP}$).

Beyond this general structure there are a number of interesting features. Note that as M'_1 increases the LSP mass first increases reaching a maximum of ~ 560 GeV at $M'_1 \sim 800$ GeV and then falls down crossing all possible s -channel resonances twice. Starting from $M'_1 = 0$ we first arrive at a little dip in the relic density around $M'_1 = 250$ GeV which is due to the s -channel H_2/A resonance. The next resonance due to Z_2/H_3 around $M'_1 = 500$ GeV produces only a little wiggle since the LSP has not yet developed an appreciable singlino component. The first appreciable dip in the relic density occurs around $M'_1 = 0.8$ TeV where $\Omega_{CDM}h^2$ drops to ~ 0.02 . Here the LSP has a strong higgsino component which enhances the annihilation via the s -channel Z_2/H_3 resonances considerably. Increasing M'_1 further, the LSP mass increases, going off-resonance (hence local maximum in the relic density), until it reaches its maximum of ~ 590 GeV at $M'_1 \sim 800$ GeV. From now on the LSP mass decreases and its nature becomes singlino-dominated. Around $M'_1 = 1.5$ TeV it once again hits the Z_2/H_3 resonance. However, this time the LSP is predominantly singlino. Although pure singlino neutralinos do not couple to the singlet Higgs, so the H_3 resonance is subdominant, they couple strongly to

the Z' and annihilate very efficiently. As a result, the relic density drops to $\sim 2 \times 10^{-3}$.

The next feature of interest is the kink at $M'_1 = 2.5$ TeV. This is where the LSP mass drops below threshold for production of $H_1 A$ in the final state. This backs up our expectation that annihilation to heavier Higgs states significantly increases the annihilation rate of a singlino LSP.

From this point on the relic density profile shows the same essential features as in Scenario A. We find a pseudoscalar Higgs resonance at $M'_1 = 3.5$ TeV, the top threshold at $M'_1 = 5$ TeV, the light Higgs threshold at $M'_1 = 11$ TeV, the light Higgs resonance at $M'_1 = 14$ TeV and the Z resonance at $M'_1 = 19$ TeV. The one important difference that is worth noting is that in this figure the light Higgs resonance does lower the relic density to a point where it agrees with the WMAP-5 measurements. This is due to the doubling of λ between the two cases. This strengthens the coupling of the singlino-higgsino-higgs vertex.

In our study of Scenario B we can clearly see the effects of increasing the size of μ . We can have a heavier singlino which can annihilate to a wider range of final states. The singlino also has stronger couplings to the other Higgs and higgsino states, further reducing the relic density. However we see once again that we need to tune the mass of the singlino through M'_1 to fit the relic density, either through a precise balance of the singlino/higgsino mixture, or through a careful balance of the singlino mass against the mass of a boson that mediates annihilation in the s-channel.

5.3.3 Direct detection

In Fig. 12 the spin-independent as well as spin-dependent elastic cross section of the lightest neutralino on proton is shown as a function of M'_1 . We restrict the range of M'_1 to 0–3 TeV, as beyond this range the cross section falls monotonically.

Referring to Fig. (10), it is easy to understand the M'_1 behavior of the cross section. For small M'_1 the lightest neutralino (up to $M'_1 \sim 0.3$ TeV) is almost a pure MSSM bino and its couplings are roughly M'_1 -independent. As M'_1 approaches 500 GeV, the LSP receives an appreciable admixture of both higgsinos. As a result both spin-independent and spin-dependent cross sections rise. However, the spin-dependent cross section being sensitive to the combination c_{34} develops a dip around $M'_1 = 800$ GeV until the discontinuity where two lightest states cross. Above 800 GeV the steady increase of the singlino component in the LSP makes the behavior of the cross section resemble the one in the previous scenario (for $M'_1 > 2.5$ TeV).

6 Summary and conclusions

In this paper we have provided an up to date and comprehensive analysis of neutralino dark matter within the USSM which contains, in addition to the MSSM states, also

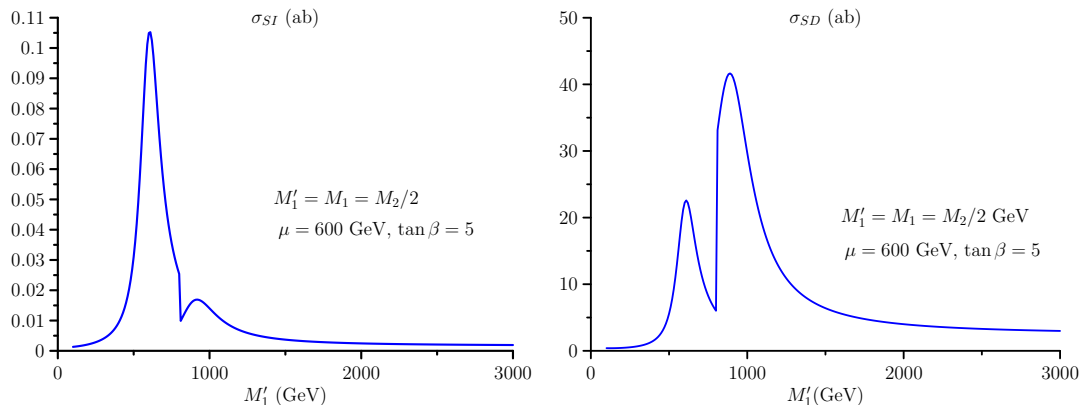


Figure 12: *The elastic spin-independent (left) and spin-dependent (right) LSP-proton cross section as a function of M'_1 in the unified scenario $M'_1 = M_1$.*

one additional singlet Higgs plus an extra Z' , together with their superpartners the singlino and bino'. We have seen that the extra states of the USSM can significantly modify the nature and properties of neutralino dark matter relative to that of the MSSM and NMSSM. Using the LanHEP package, we have derived all the new Feynman rules relevant for the dark matter calculations. We have also provided a complete qualitative discussion of the new annihilation channels relevant for the calculation of the cold dark matter relic density for the neutralino LSP in the USSM. We also discussed the elastic scattering cross section for the neutralino LSP in the USSM, including both spin-independent and spin-dependent parts of the cross sections, relevant for the direct dark matter search experiments.

We then surveyed the parameter space of the USSM, and discussed quantitatively how the nature and composition of the neutralino LSP can be significantly altered compared to that in the MSSM due to the extra singlino and bino' states, for different ranges of parameters. We have considered two approaches to the parameter space: (a) holding the MSSM higgsino and gaugino mass parameters fixed, while the mass of the extra U(1) gaugino taken free (to complement the collider phenomenology discussed in Ref. [18]); (b) the scenario of unified gaugino masses. The Feynman rules were then implemented into the micrOMEGAs package in order to calculate the relic density for the corresponding regions of parameter space. This provides a full calculation of the annihilation channels including co-annihilation and careful treatment of resonances as well as accurately calculating the relic density for an arbitrary admixture of states. In this way we extended the analysis of USSM dark matter annihilation beyond the specific cases previously studied in the literature. We also performed an equally general calculation of the direct detection cross-sections for USSM dark matter for elastic neutralino–nuclei scattering.

The results show that there are many cases where successful relic abundances may be achieved, and in novel ways compared to the MSSM or NMSSM (see for example the low mass region in Fig. 11 for $M'_1 < 5$ TeV). In general our results also show that the inclusion of the bino' state, as well as the lack of a cubic interaction term \hat{S}^3 , results in a significant change in the dark matter phenomenology of the USSM as compared to that of MSSM or NMSSM. Also the neutralino mass spectrum in the USSM may be very different from that of the NMSSM as the singlino mass is determined indirectly by a mini-see-saw mechanism involving the bino' soft mass parameter M'_1 rather than through a diagonal mass term arising from the cubic \hat{S}^3 . The lack of a cubic interaction term also restricts the annihilation modes of the singlino, making it dominantly reliant on annihilations involving non-singlet Higgs bosons and higgsinos. As the USSM has a different Higgs spectrum to the NMSSM, notably in the pseudoscalar Higgs sector, the Higgs dominated annihilation channels of the USSM singlino are significantly modified with respect to the NMSSM singlino. As Higgs exchange diagrams dominate the direct detection phenomenology, the difference in the Higgs spectrum and the singlino interactions results in significant differences in the direct detection predictions as well.

In conclusion, the USSM, despite its modest additional particle content compared to the MSSM or NMSSM, leads to a surprisingly rich and interesting dark matter phenomenology which distinguishes it from these models. The other states which are necessary in order to make the model anomaly free, and which we have neglected here, can only add to the richness of the resulting phenomenology, but the qualitatively new features that we have found in the USSM will remain in any more complete model. Nevertheless it would be interesting to study the effect of the additional states present, for example, in the E_6 SSM in a future study.

Acknowledgments

JK was partially supported by the Polish Ministry of Science and Higher Education Grant No 1 P03B 108 30. This research was supported by the EC Programme MTKD-CT-2005-029466 "Particle Physics and Cosmology: the Interface", the EU Network MRTN-CT-2006-035505 "Tools and Precision Calculations for Physics Discoveries at Colliders"; STFC Rolling Grant PPA/G/S/2003/00096; EU Network MRTN-CT-2004-503369; EU ILIAS RII3-CT-2004-506222; NSF CAREER grant PHY-0449818 and DOE OJI grant # DE-FG02-06ER41417. JPR would like to thank Yosi Gelfand and Neal Weiner for useful discussions. The authors would also like to thank Dorota Jarecka for collaboration in the early stage of this work.

A Higgs boson masses

In general the neutral CP-even Higgs fields h, H, S mix. The mass matrix takes the form (see the first paper in [27])

$$M_{even}^2 = \begin{pmatrix} M_{11}^2 & M_{12}^2 & M_{13}^2 \\ M_{21}^2 & M_{22}^2 & M_{23}^2 \\ M_{31}^2 & M_{32}^2 & M_{33}^2 \end{pmatrix} \quad (\text{A.1})$$

where

$$\begin{aligned} M_{11}^2 &= \frac{\lambda^2}{2} v^2 \sin^2 2\beta + \frac{g'^2 + g_2^2}{4} v^2 \cos^2 2\beta + g_1'^2 v^2 (Q_1 \cos^2 \beta + Q_2 \sin^2 \beta)^2 + \Delta_{11}, \\ M_{12}^2 &= M_{21}^2 = \left(\frac{\lambda^2}{4} - \frac{g'^2 + g_2^2}{8} \right) v^2 \sin 4\beta + \frac{g_1'^2}{2} v^2 (Q_2 - Q_1) \times \\ &\quad \times (Q_1 \cos^2 \beta + Q_2 \sin^2 \beta) \sin 2\beta + \Delta_{12}, \\ M_{22}^2 &= \frac{\sqrt{2} \lambda A_\lambda}{\sin 2\beta} v_S + \left(\frac{g'^2 + g_2^2}{4} - \frac{\lambda^2}{2} \right) v^2 \sin^2 2\beta + \frac{g_1'^2}{4} (Q_2 - Q_1)^2 v^2 \sin^2 2\beta + \Delta_{E22}, \\ M_{13}^2 &= M_{31}^2 = -\frac{\lambda A_\lambda}{\sqrt{2}} v \sin 2\beta + \lambda^2 v v_S + g_1'^2 (Q_1 \cos^2 \beta + Q_2 \sin^2 \beta) Q_S v v_S + \Delta_{13}, \\ M_{23}^2 &= M_{32}^2 = -\frac{\lambda A_\lambda}{\sqrt{2}} v \cos 2\beta + \frac{g_1'^2}{2} (Q_2 - Q_1) Q_S' v v_S \sin 2\beta + \Delta_{23}, \\ M_{33}^2 &= \frac{\lambda A_\lambda}{2\sqrt{2} v_S} v^2 \sin 2\beta + g_1'^2 Q_S^2 v_S^2 + \Delta_{E33} \end{aligned} \quad (\text{A.2})$$

where the one loop-corrections Δ_{Eij} are expressed as

$$\begin{aligned} \Delta_{E22} &= \Delta_{22} + \Delta_A - \Delta_\beta \\ \Delta_{E33} &= \Delta_{33} - \frac{\Delta_S}{v_S} \\ \Delta_{EA} &= \Delta_A - \Delta_\beta - \frac{\Delta_S}{v_S} + \Delta_3 \end{aligned} \quad (\text{A.3})$$

in terms of Δ_{ij} , Δ_S , Δ_β , Δ_A and Δ_3 given explicitly in Ref. [33] (note that the expression for K in this paper should read $K = F - \frac{1}{2} \log \frac{m_{t_1}^2 m_{t_2}^2}{Q^4}$).

B Feynman rules

All the Feynman rules presented here are given in terms of the interaction of mass eigenstates. As a result the Feynman rules reference many matrices that rotate from the interaction eigenstate to the mass eigenstate basis. We briefly summarise them here for ease of reference:

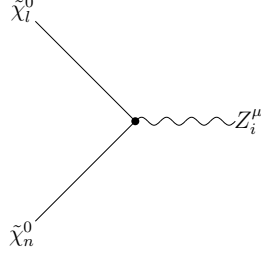


Figure B.1: The $Z_i^\mu \tilde{\chi}_l^0 \tilde{\chi}_n^0$ vertex given in Eq. (B.1)

- D_{ij} - Z, Z' mixing matrix that transforms from the Z, Z' eigenstates to the $Z_{1,2}$ mass eigenstates, as defined in Eq. (10)
- \mathcal{O}'_{ij} - Higgs mixing matrix from the mass eigenstate basis to the the interaction eigenstate basis, defined in Eq. (18).
- N_{ij} - neutralino mixing matrix, defined in Eq. (26)
- U_{ij}, V_{ij} - standard chargino mixing matrices as in the MSSM [4].
- $U_{\tilde{f}}^{ij}$ - squark or slepton mixing matrix, defined in Eq. (31).

Feynman rule for the $Z_i^\mu \tilde{\chi}_l^0 \tilde{\chi}_n^0$ vertex shown in Fig. B.1:

$$\begin{aligned}
i\gamma_\mu & \left[P_L \left\{ \frac{D_{iZ}g_2}{2 \cos \theta_W} (-N_{l3}N_{n3}^* + N_{l4}N_{n4}^*) \right. \right. \\
& \quad \left. \left. - D_{iZ'}g_1' (Q_1N_{l3}N_{n3}^* + Q_2N_{l4}N_{n4}^* + Q_S N_{l5}N_{n5}^*) \right\} \right. \\
& \quad \left. - P_R \left\{ \frac{D_{iZ}g_2}{2 \cos \theta_W} (-N_{l3}^*N_{n3} + N_{l4}^*N_{n4}) \right. \right. \\
& \quad \left. \left. - D_{iZ'}g_1' (Q_1N_{l3}^*N_{n3} + Q_2N_{l4}^*N_{n4} + Q_S N_{l5}^*N_{n5}) \right\} \right] \quad (B.1)
\end{aligned}$$

Feynman rules for the $\tilde{\chi}_k^\pm \tilde{\chi}_l^0 W_\mu^\mp$ vertex shown in Fig. B.2

$$i g_2 \gamma^\mu (C_{lk}^L P_L + C_{lk}^R P_R) \quad (B.2)$$

$$i g_2 \gamma^\mu (C_{lk}^{R*} P_L + C_{lk}^{L*} P_R) \quad (B.3)$$

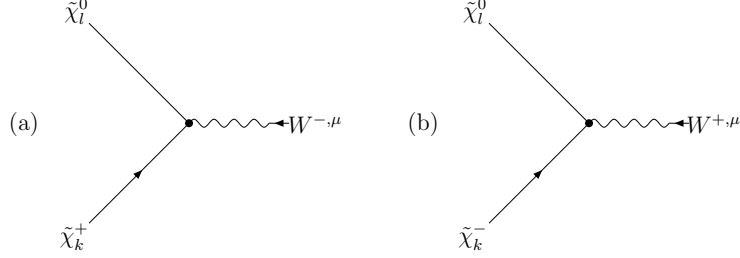


Figure B.2: The $\tilde{\chi}_k^\pm \tilde{\chi}_l^0 W_\mu^\mp$ vertex given in (a) Eq. (B.2) and (b) Eq. (B.3)

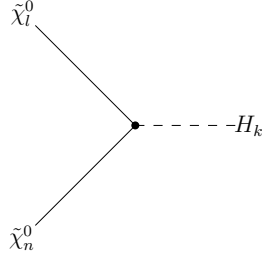


Figure B.3: The $\tilde{\chi}_l^0 \tilde{\chi}_n^0 H_k$ vertex given in Eq. (B.6)

where

$$C_{lk}^L = N_{l2} V_{k1}^* - \frac{1}{\sqrt{2}} N_{l4} V_{k2}^* \quad (\text{B.4})$$

$$C_{lk}^R = N_{l2}^* U_{k1} - \frac{1}{\sqrt{2}} N_{l3}^* U_{k2} \quad (\text{B.5})$$

Feynman rule for the $\tilde{\chi}_l^0 \tilde{\chi}_n^0 H_k$ vertex shown in Fig. B.6:

$$i (\mathcal{O}'_{1k} R_{ln}^* + \mathcal{O}'_{2k} S_{ln}^* + \mathcal{O}'_{3k} T_{ln}^*) P_L + (\mathcal{O}'_{1k} R_{nl} + \mathcal{O}'_{2k} S_{nl} + \mathcal{O}'_{3k} T_{nl}) P_R \quad (\text{B.6})$$

where

$$R_{nl} = -\frac{g_2}{2} (N_{n2} - \tan \theta_W N_{n1}) N_{l3} - g'_1 Q_1 N_{n6} N_{l3} + \frac{\lambda}{\sqrt{2}} N_{n4} N_{l5} + (l \leftrightarrow n) \quad (\text{B.7})$$

$$S_{nl} = \frac{g_2}{2} (N_{n2} - \tan \theta_W N_{n1}) N_{l4} - g'_1 Q_2 N_{n6} N_{l4} + \frac{\lambda}{\sqrt{2}} N_{n3} N_{l5} + (l \leftrightarrow n) \quad (\text{B.8})$$

$$T_{nl} = -g'_1 Q_S N_{n6} N_{l5} + \frac{\lambda}{\sqrt{2}} N_{n3} N_{l4} + (l \leftrightarrow n) \quad (\text{B.9})$$

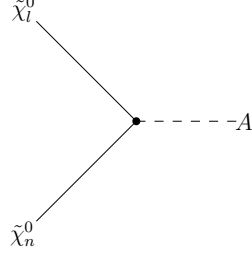


Figure B.4: The $\tilde{\chi}_l^0 \tilde{\chi}_n^0 A$ vertex given in Eq. (B.10)

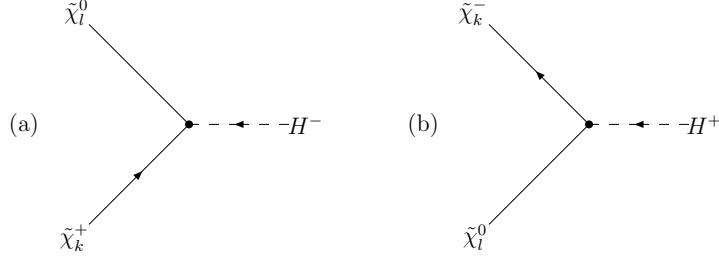


Figure B.5: The $\tilde{\chi}_k^\pm \tilde{\chi}_l^0 H^\mp$ vertex given in (a) Eq. (B.14) and (b) Eq. (B.15)

Feynman rule for the $\tilde{\chi}_l^0 \tilde{\chi}_n^0 A$ vertex shown in Fig. B.10:

$$\begin{aligned}
 & [(R'_{ln} \sin \beta + S'_{ln} \cos \beta) \cos \phi + T'_{ln} \sin \phi] P_L \\
 & - [(R'_{nl} \sin \beta + S'_{nl} \cos \beta) \cos \phi + T'_{nl} \sin \phi] P_R
 \end{aligned} \tag{B.10}$$

where

$$\begin{aligned}
 R'_{nl} &= -\frac{g_2}{2} (N_{l2} - \tan \theta_W N_{l1}) N_{n3} - g'_1 Q_1 N_{l3} N_{n6} - \frac{\lambda}{\sqrt{2}} N_{l4} N_{n5} \\
 &+ (l \leftrightarrow n)
 \end{aligned} \tag{B.11}$$

$$\begin{aligned}
 S'_{nl} &= \frac{g_2}{2} (N_{l2} - \tan \theta_W N_{l1}) N_{n4} - g'_1 Q_2 N_{l4} N_{n6} - \frac{\lambda}{\sqrt{2}} N_{l3} N_{n5} \\
 &+ (l \leftrightarrow n)
 \end{aligned} \tag{B.12}$$

$$T'_{nl} = -g'_1 Q_S N_{l5} N_{n6} - \frac{\lambda}{\sqrt{2}} N_{l3} N_{n4} \tag{B.13}$$

Feynman rules for $\tilde{\chi}_k^\pm \tilde{\chi}_l^0 H^\mp$ shown in Fig. B.5:

$$-i \left(R''_{lk}{}^L P_L + R''_{lk}{}^R P_R \right) \tag{B.14}$$

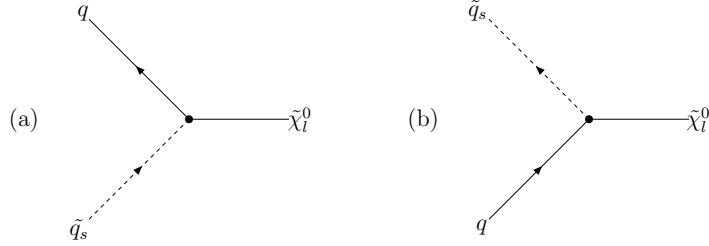


Figure B.6: The $q\tilde{q}_s\tilde{\chi}_l^0$ vertex given in (a) Eq. (B.18) and (b) Eq. (B.19)

$$-i \left(R''_{lk}{}^{R*} P_L + R''_{lk}{}^{L*} P_R \right) \quad (\text{B.15})$$

where

$$R''_{lk}{}^{L} = g_2 \cos \beta \left[N_{l4}^* V_{k1}^* + \frac{V_{k2}^*}{\sqrt{2}} (N_{l2}^* + N_{l1}^* \tan \theta_W) \right] + g'_1 \sqrt{2} \cos \beta Q_2 N_{l6}^* V_{k2}^* + \lambda \sin \beta N_{l5}^* V_{k2}^* \quad (\text{B.16})$$

$$R''_{lk}{}^{R} = g_2 \sin \beta \left[N_{l3} U_{k1} - \frac{U_{k2}}{\sqrt{2}} (N_{l2} - N_{l1} \tan \theta_W) \right] + g'_1 \sqrt{2} \sin \beta Q_1 N_{l6} U_{k2} + \lambda \cos \beta N_{l5} U_{k2} \quad (\text{B.17})$$

Feynman rules for the $q\tilde{q}_s\tilde{\chi}_l^0$ vertex shown in Fig. B.6:

$$i [(G_{sl}^{qL})^* P_R + (G_{sl}^{qR})^* P_L] \quad (\text{B.18})$$

$$i [G_{sl}^{qL} P_L + G_{sl}^{qR} P_R] \quad (\text{B.19})$$

For up-type quarks:

$$G_{sl}^{uL} = -\sqrt{2} \left[g_2 \left(\frac{1}{2} N_{l2}^* + \frac{1}{6} \tan \theta_W N_{l1}^* \right) + g'_1 Q_Q N_{l6}^* \right] U_{\tilde{u}_i}^{1s} - \frac{g_2 m_{u_i}}{\sqrt{2} M_W \sin \beta} N_{l4}^* U_{\tilde{u}_i}^{2s}$$

$$G_{sl}^{uR} = \sqrt{2} \left[g_2 \frac{2}{3} \tan \theta_W N_{l1} - g'_1 Q_{\bar{u}} N_{l6} \right] U_{\tilde{u}_i}^{2s} - \frac{g_2 m_{u_i}}{\sqrt{2} M_W \sin \beta} N_{l4} U_{\tilde{u}_i}^{1s} \quad (\text{B.20})$$

For down-type quarks:

$$G_{sl}^{dL} = \sqrt{2} \left[g_2 \left(\frac{1}{2} N_{l2}^* - \frac{1}{6} \tan \theta_W N_{l1}^* \right) - g'_1 Q_Q N_{l6}^* \right] U_{\tilde{d}_i}^{1s} - \frac{g_2 m_{d_i}}{\sqrt{2} M_W \cos \beta} N_{l3}^* U_{\tilde{d}_i}^{2s}$$

$$G_{sl}^{dR} = -\sqrt{2} \left[\frac{1}{6} \tan \theta_W N_{l1} + g'_1 Q_{\bar{d}} N_{l6} \right] U_{\tilde{d}_i}^{2s} - \frac{g_2 m_{d_i}}{\sqrt{2} M_W \cos \beta} N_{l3} U_{\tilde{d}_i}^{1s} \quad (\text{B.21})$$

References

- [1] J. Ellis, J.S. Hagelin, D.V. Nanopoulos, K.A. Olive and M. Srednicki, Nucl. Phys. B **238** (1984) 453; see also H. Goldberg, Phys. Rev. Lett. **50** (1983) 1419.
- [2] G. Jungman, M. Kamionkowski and K. Griest, Phys. Rept. **267** (1996) 195 [arXiv:hep-ph/9506380].
- [3] J. Dunkley *et al.* [WMAP Collaboration], arXiv:0803.0586 [astro-ph].
- [4] For a review see e.g. D. J. H. Chung, L. L. Everett, G. L. Kane, S. F. King, J. D. Lykken and L. T. Wang, Phys. Rept. **407** (2005) 1 [arXiv:hep-ph/0312378].
- [5] G. L. Kane and S. F. King, Phys. Lett. B **451** (1999) 113 [arXiv:hep-ph/9810374];
- [6] J. E. Kim and H. P. Nilles, Phys. Lett. B **138** (1984) 150. For a recent discussion of the μ problem see T. Cohen and A. Pierce, arXiv:0803.0765 [hep-ph].
- [7] M. Bastero-Gil, C. Hugonie, S. F. King, D. P. Roy and S. Vempati, Phys. Lett. B **489** (2000) 359 [arXiv:hep-ph/0006198]; E. Keith and E. Ma, Phys. Rev. D **54** (1996) 3587 [arXiv:hep-ph/9603353]; E. Ma, Phys. Rev. Lett. **60** (1988) 1363.
- [8] R. D. Peccei and H. R. Quinn, Phys. Rev. Lett. **38**, 1440 (1977). R. D. Peccei and H. R. Quinn, Phys. Rev. D **16**, 1791 (1977).
- [9] P. Fayet, Nucl. Phys. B **78** (1974) 14; P. Fayet, Nucl. Phys. B **90** (1975) 104; P. Fayet, Phys. Lett. B **64** (1976) 159.
- [10] H. P. Nilles, M. Srednicki and D. Wyler, Phys. Lett. B **120** (1983) 346; J. M. Frere, D. R. T. Jones and S. Raby, Nucl. Phys. B **222**, 11 (1983); J. P. Derendinger and C. A. Savoy, Nucl. Phys. B **237** (1984) 307; J. R. Ellis, J. F. Gunion, H. E. Haber, L. Roszkowski and F. Zwirner, Phys. Rev. D **39**, 844 (1989); S. F. King and P. L. White, Phys. Rev. D **52**, 4183 (1995) [arXiv:hep-ph/9505326]; S. F. King and P. L. White, Phys. Rev. D **53**, 4049 (1996) [arXiv:hep-ph/9508346]. For a recent summary and references, see e.g. D.J. Miller, R. Nevzorov and P.M. Zerwas, Nucl. Phys. B **681** (2004) 3; A. Djouadi *et al.*, JHEP **0807** (2008) 002 arXiv:0801.4321 [hep-ph].
- [11] C. Panagiotakopoulos and K. Tamvakis, Phys. Lett. B **446** (1999) 224 [arXiv:hep-ph/9809475].
- [12] C. Panagiotakopoulos and K. Tamvakis, Phys. Lett. B **469** (1999) 145 [arXiv:hep-ph/9908351].
- [13] P. Fayet, Phys. Lett. B **69** (1977) 489.

- [14] D. Suematsu and Y. Yamagishi, *Int. J. Mod. Phys. A* **10** (1995) 4521.
- [15] B. de Carlos and J. R. Espinosa, *Phys. Lett. B* **407** (1997) 12 [arXiv:hep-ph/9705315].
- [16] M. Cvetič, D. A. Demir, J. R. Espinosa, L. L. Everett and P. Langacker, *Phys. Rev. D* **56** (1997) 2861 [Erratum-ibid. *D* **58** (1998) 119905] [arXiv:hep-ph/9703317].
- [17] V. Barger, P. Langacker and G. Shaughnessy, *Phys. Lett. B* **644** (2007) 361 [arXiv:hep-ph/0609068]; V. Barger, P. Langacker, H. S. Lee and G. Shaughnessy, *Phys. Rev. D* **73** (2006) 115010 [arXiv:hep-ph/0603247]; V. Barger, P. Langacker and G. Shaughnessy, *New J. Phys.* **9** (2007) 333 [arXiv:hep-ph/0702001]; V. Barger, P. Langacker, M. McCaskey, M. J. Ramsey-Musolf and G. Shaughnessy, *Phys. Rev. D* **77** (2008) 035005 arXiv:0706.4311 [hep-ph].
- [18] S. Y. Choi, H. E. Haber, J. Kalinowski and P. M. Zerwas, *Nucl. Phys. B* **778** (2007) 85 [arXiv:hep-ph/0612218], and references therein.
- [19] V. Barger, P. Langacker, I. Lewis, M. McCaskey, G. Shaughnessy and B. Yencho, *Phys. Rev. D* **75** (2007) 115002 [arXiv:hep-ph/0702036].
- [20] D. Jarecka, J. Kalinowski, S. F. King and J. P. Roberts, *In the Proceedings of 2007 International Linear Collider Workshop (LCWS07 and ILC07), Hamburg, Germany, 30 May - 3 Jun 2007, pp SUS15* [arXiv:0709.1862 [hep-ph]]; *J. Phys. Conf. Ser.* **110**, 072019 (2008).
- [21] O. Adriani *et al.*, arXiv:0810.4995 [astro-ph]; M. Boezio *et al.*, arXiv:0810.3508 [astro-ph].
- [22] N. Arkani-Hamed, D. P. Finkbeiner, T. Slatyer and N. Weiner, arXiv:0810.0713 [hep-ph]; I. Cholis, D. P. Finkbeiner, L. Goodenough and N. Weiner, arXiv:0810.5344 [astro-ph]; I. Cholis, L. Goodenough, D. Hooper, M. Simet and N. Weiner, arXiv:0809.1683 [hep-ph]; M. Cirelli, M. Kadastik, M. Raidal and A. Strumia, arXiv:0809.2409 [hep-ph]; L. Bergstrom, T. Bringmann and J. Edsjo, arXiv:0808.3725 [astro-ph]; M. Cirelli and A. Strumia, arXiv:0808.3867 [astro-ph]; J. H. Huh, J. E. Kim and B. Kyae, arXiv:0809.2601 [hep-ph]; V. Barger, W. Y. Keung, D. Marfatia and G. Shaughnessy, arXiv:0809.0162 [hep-ph]; C. R. Chen, F. Takahashi and T. T. Yanagida, arXiv:0809.0792 [hep-ph]; C. R. Chen and F. Takahashi, arXiv:0810.4110 [hep-ph]; M. Fairbairn and J. Zupan, arXiv:0810.4147 [hep-ph].
- [23] H. Yuksel, M. D. Kistler and T. Stanev, arXiv:0810.2784 [astro-ph]; D. Hooper, P. Blasi and P. D. Serpico, arXiv:0810.1527 [astro-ph]; I. Buesching, O. C. de Jager, M. S. Potgieter and C. Venter, arXiv:0804.0220 [astro-ph]; L. Zhang and

- K. S. Cheng, *Astron. Astrophys.* **368**, 1063 (2001). X. Chi, E. C. M. Young and K. S. Cheng, *Astrophys. J.* **459**, L83 (1995).
- [24] A. Semenov, arXiv:0805.0555 [hep-ph]; A. V. Semenov, arXiv:hep-ph/0208011.
- [25] G. Belanger, F. Boudjema, A. Pukhov and A. Semenov, arXiv:0803.2360 [hep-ph]; G. Belanger, F. Boudjema, A. Pukhov and A. Semenov, *Comput. Phys. Commun.* **176**, 367 (2007) [arXiv:hep-ph/0607059]; G. Belanger, F. Boudjema, A. Pukhov and A. Semenov, *Comput. Phys. Commun.* **174** (2006) 577 [arXiv:hep-ph/0405253]; G. Belanger, F. Boudjema, A. Pukhov and A. Semenov, arXiv:hep-ph/0112278.
- [26] E. Keith and E. Ma, *Phys. Rev. D* **56** (1997) 7155 [arXiv:hep-ph/9704441].
- [27] S. F. King, S. Moretti and R. Nevzorov, *Phys. Rev. D* **73** (2006) 035009 [arXiv:hep-ph/0510419]; S. F. King, S. Moretti and R. Nevzorov, *Phys. Lett. B* **634** (2006) 278 [arXiv:hep-ph/0511256]; S. F. King, S. Moretti and R. Nevzorov, *Phys. Lett. B* **650** (2007) 57 [arXiv:hep-ph/0701064]; R. Howl and S. F. King, *Phys. Lett. B* **652** (2007) 331 arXiv:0705.0301 [hep-ph]; R. Howl and S. F. King, arXiv:0708.1451 [hep-ph];
- [28] B. Holdom, *Phys. Lett. B* **166** (1986) 196.
- [29] F. del Aguila, *Acta. Phys. Pol. B* **25** (1994) 1317 [hep-ph/9404323]; F. del Aguila, M. Cvetič and P. Langacker, *Phys. Rev. D* **52** (1995) 37 [hep-ph/9501390]; K.S. Babu, C. Kolda and J. March–Russell, *Phys. Rev. D* **54** (1996) 4635 [hep-ph/9603212]; K.R. Dienes, C. Kolda, J. March–Russell, *Nucl. Phys. B* **492** (1997) 104 [hep-ph/9610479]; D. Suematsu, *Phys. Rev. D* **59** (1999) 055017 [hep-ph/9808409].
- [30] P. Langacker, arXiv:0801.1345 [hep-ph].
- [31] P. Abreu *et al.* [DELPHI Collaboration], *Phys. Lett. B* **485** (2000) 45; R. Barate *et al.* [ALEPH Collaboration], *Eur. Phys. J. C* **12** (2000) 183; A. Abulencia *et al.* [CDF Collaboration], hep-ph/0602045.
- [32] A. Brignole, J. Ellis, G. Ridolfi, F. Zwirner, *Phys. Lett. B* **271** (1991) 123; P. H. Chankowski, S. Pokorski, J. Rosiek, *Phys. Lett. B* **274** (1992) 191; A. Brignole, *Phys. Lett. B* **277** (1992) 313; H. E. Haber, R. Hempfling, *Phys. Rev. D* **48** (1993) 4280.
- [33] P. A. Kovalenko, R. B. Nevzorov and K. A. Ter-Martirosian, *Phys. Atom. Nucl.* **61**, 812 (1998) [*Yad. Fiz.* **61**, 898 (1998)].
- [34] D. Suematsu, *JHEP* **0611** (2006) 029 [arXiv:hep-ph/0606125].

- [35] T. Takagi, Japan J. Math. **1** (1925) 83. R.A. Horn and C.R. Johnson, *Matrix Analysis* (Cambridge University Press, Cambridge, England, 1990). A. Bunse-Gerstner and W.B. Gragg, J. Comp. Appl. Math. **21** (1988) 41. W. Xu and S. Qiao, Technical Report No. CAS 05-01-SQ (2005). X. Wang and S. Qiao, Proc. Int. Conference on Parallel and Distributed Processing Techniques and Applications, Vol. I, edited by H.R. Arabnia, pp. 206-212 (2002). F.T. Luk and S. Qiao, Proc. SPIE **4474** (2001) 254. T. Hahn, arXiv:physics/0607103.
- [36] J. R. Ellis and K. A. Olive, Phys. Lett. B **514** (2001) 114 [arXiv:hep-ph/0105004]; J. R. Ellis, K. A. Olive and Y. Santoso, New J. Phys. **4** (2002) 32 [arXiv:hep-ph/0202110]; J. R. Ellis, S. Heinemeyer, K. A. Olive and G. Weiglein, JHEP **0502** (2005) 013 [arXiv:hep-ph/0411216]; S. F. King and J. P. Roberts, JHEP **0609** (2006) 036 [arXiv:hep-ph/0603095]; S. F. King and J. P. Roberts, Acta Phys. Polon. B **38** (2007) 607 [arXiv:hep-ph/0609147]; S. F. King and J. P. Roberts, JHEP **0701** (2007) 024 [arXiv:hep-ph/0608135]; S. F. King, J. P. Roberts and D. P. Roy, JHEP **0710** (2007) 106 arXiv:0705.4219 [hep-ph]; M. Battaglia, A. De Roeck, J. R. Ellis, F. Gianotti, K. A. Olive and L. Pape, Eur. Phys. J. C **33** (2004) 273 [arXiv:hep-ph/0306219]; E. A. Baltz, M. Battaglia, M. E. Peskin and T. Wizansky, Phys. Rev. D **74** (2006) 103521 [arXiv:hep-ph/0602187]; J. Ellis, S. F. King and J. P. Roberts, JHEP **0804** (2008) 099 arXiv:0711.2741 [hep-ph];
- [37] G. L. Kane, C. F. Kolda, L. Roszkowski and J. D. Wells, Phys. Rev. D **49** (1994) 6173 [arXiv:hep-ph/9312272]; J. R. Ellis, T. Falk, K. A. Olive and M. Srednicki, Astropart. Phys. **13** (2000) 181 [Erratum-ibid. **15** (2001) 413] [arXiv:hep-ph/9905481]; J. Ellis, T. Falk and K. A. Olive, Phys. Lett. B **444** (1998) 367 [arXiv:hep-ph/9810360]; M. E. Gómez, G. Lazarides and C. Pallas, Phys. Rev. D **61** (2000) 123512 [arXiv:hep-ph/9907261]; Phys. Lett. B **487** (2000) 313 [arXiv:hep-ph/0004028] and Nucl. Phys. B **638** (2002) 165 [arXiv:hep-ph/0203131]; T. Nihei, L. Roszkowski and R. Ruiz de Austri, JHEP **0207** (2002) 024 [arXiv:hep-ph/0206266]; S. Mizuta and M. Yamaguchi, Phys. Lett. B **298** (1993) 120 [arXiv:hep-ph/9208251]; J. Edsjo and P. Gondolo, Phys. Rev. D **56** (1997) 1879 [arXiv:hep-ph/9704361]; A. Birkedal-Hansen and E. Jeong, arXiv:hep-ph/0210041; H. Baer, C. Balazs and A. Belyaev, JHEP **0203**, 042 (2002) [arXiv:hep-ph/0202076]; J. R. Ellis, T. Falk, G. Ganis, K. A. Olive and M. Srednicki, Phys. Lett. B **510** (2001) 236 [arXiv:hep-ph/0102098]; J. R. Ellis, K. A. Olive and Y. Santoso, New Jour. Phys. **4** (2002) 32 [arXiv:hep-ph/0202110]; M. Drees and M. M. Nojiri, Phys. Rev. D **47** (1993) 376 [arXiv:hep-ph/9207234]; H. Baer and M. Brhlik, Phys. Rev. D **53** (1996) 597 [arXiv:hep-ph/9508321] and Phys. Rev. D **57** (1998) 567 [arXiv:hep-ph/9706509]; H. Baer, M. Brhlik, M. A. Diaz, J. Ferrandis, P. Mercadante, P. Quintana and X. Tata, Phys. Rev. D **63** (2001) 015007 [arXiv:hep-ph/0005027]; A. B. Lahanas, D. V. Nanopoulos and V. C. Spanos, Mod.

- Phys. Lett. A **16** (2001) 1229 [arXiv:hep-ph/0009065]; J. R. Ellis, D. V. Nanopoulos and K. A. Olive, Phys. Lett. B **525** (2002) 308 [arXiv:hep-ph/0109288]; J. R. Ellis, T. Falk, K. A. Olive and M. Schmitt, Phys. Lett. B **388** (1996) 97 [arXiv:hep-ph/9607292]; J. L. Feng, K. T. Matchev and T. Moroi, Phys. Rev. Lett. **84** (2000) 2322 [arXiv:hep-ph/9908309]; J. L. Feng, K. T. Matchev and T. Moroi, Phys. Rev. D **61** (2000) 075005 [arXiv:hep-ph/9909334]; J. L. Feng, K. T. Matchev and F. Wilczek, Phys. Lett. B **482** (2000) 388 [arXiv:hep-ph/0004043]; J. L. Feng, K. T. Matchev and F. Wilczek, Phys. Lett. B **482** (2000) 388 [arXiv:hep-ph/0004043]; K. Griest and D. Seckel, Phys. Rev. D **43** (1991) 3191; J. R. Ellis, T. Falk, K. A. Olive and M. Srednicki, Astropart. Phys. **13** (2000) 181 [Erratum-ibid. **15** (2001) 413] [arXiv:hep-ph/9905481].
- [38] S. Kraml, A. R. Raklev and M. J. White, arXiv:0811.0011 [hep-ph], C. Hugonie, G. Belanger and A. Pukhov, JCAP **0711** (2007) 009 arXiv:0707.0628 [hep-ph], D. G. Cerdeno, E. Gabrielli, D. E. Lopez-Fogliani, C. Munoz and A. M. Teixeira, JCAP **0706** (2007) 008 [arXiv:hep-ph/0701271], J. F. Gunion, D. Hooper and B. McElrath, Phys. Rev. D **73** (2006) 015011 [arXiv:hep-ph/0509024], G. Belanger, F. Boudjema, C. Hugonie, A. Pukhov and A. Semenov, JCAP **0509** (2005) 001 [arXiv:hep-ph/0505142], A. Menon, D. E. Morrissey and C. E. M. Wagner, Phys. Rev. D **70** (2004) 035005 [arXiv:hep-ph/0404184], A. Stephan, Phys. Rev. D **58** (1998) 035011 [arXiv:hep-ph/9709262], A. Stephan, Phys. Lett. B **411** (1997) 97 [arXiv:hep-ph/9704232], S. A. Abel, S. Sarkar and I. B. Whittingham, Nucl. Phys. B **392** (1993) 83 [arXiv:hep-ph/9209292], K. A. Olive and D. Thomas, Nucl. Phys. B **355** (1991) 192, R. Flores, K. A. Olive and D. Thomas, Phys. Lett. B **245** (1990) 509, B. R. Greene and P. J. Miron, Phys. Lett. B **168** (1986) 226.
- [39] DAMA/LIBRA <http://people.roma2.infn.it/dama/web/home.html>
 CDMS <http://cdms.berkeley.edu>
 XENON <http://xenen.astro.columbia.edu>
 ZEPLIN <http://www.hep.ph.ic.ac.uk/ZEPLIN-III-Project/>
 CRESST <http://www.cresst.de/cresst.php>
 WARP <http://warp.lngs.infn.it>
 COUPP <http://www-coupp.fnal.gov/>
 EDELWEISS edelweiss.in2p3.fr
- [40] EGRET <http://coss.gsfc.nasa.gov/docs/cgro/egret/>
 GLAST <http://www-glast.stanford.edu>
 HESS <http://www.mpi-hd.mpg.de/hfm/HESS/HESS.html>
 IceCube <http://www.icecube.wisc.edu/collaboration>
 KIMS <http://dmrc.snu.ac.kr>
 PAMELA <http://pamela.roma2.infn.it/index.php>
 Super-K <http://www-sk.icrr.u-tokyo.ac.jp/sk/index-e.html>

- [41] G. Jungman, M. Kamionkowski and K. Griest, Phys. Rept. **267** (1996) 195 [arXiv:hep-ph/9506380].
- [42] K. Griest, Phys. Rev. D **38** (1988) 2357 [Erratum-ibid. D **39** (1989) 3802].
- [43] M. Drees and M. Nojiri, Phys. Rev. D **48** (1993) 3483 [arXiv:hep-ph/9307208].
- [44] S. Y. Choi, S. C. Park, J. H. Jang and H. S. Song, Phys. Rev. D **64** (2001) 015006 [arXiv:hep-ph/0012370].
- [45] D. Jarecka, MSc thesis, University of Warsaw 2006 (in Polish, unpublished), <http://www.fuw.edu.pl/~djarecka/praca/praca11508dz.pdf>.
- [46] J. Ellis, K. A. Olive and C. Savage, Phys. Rev. D **77** (2008) 065026 arXiv:0801.3656 [hep-ph].